FINAL REPORT

DEVELOPMENT OF NATIONAL

PALESTINIAN GEODETIC REFERENCE FRAMEWORK

(PAL-GRF)

Reference No.: GZ-PLA-250392-CS-QCBS

January 2024

1. CONTENTS

List of Tables

List of Figures

2. ABBREVIATIONS

CORS	Continuously Operating Reference Stations
EGM	Earth's Geopotential Model
GLONASS	Globalnaya Navigazionnaya Sputnikovaya Sistema, or Global Navigation Satellite System
GNSS	Global Navigation Satellite Systems (GPS + GLONASS)
GPS	Global Positioning System
IGS	International GNSS Service
ITRF	International Terrestrial Reference Frame
CODE	Center for Orbit Determination in Europe
NNT	No Net Translation
NEQ	Normal Equations
LC	Loosely Constrained
PAL-GRF	Palestinian Geodetic Reference Framework
PLA	Palestinian Land Authority
RERP	West Bank & Gaza Real Estate Registration Project
S-Transformation	Similarity Transformation
RINEX	Receiver Independent Exchange Format
SINEX	Solution Independent Exchange Format

3. TERMS AND DEFINITIONS

Accuracy—The closeness of an estimated value (that is measured or computed) to a standard or accepted (true) value of a particular quantity.

Horizontal accuracy—The positional accuracy of a dataset with respect to a specified horizontal datum.

Vertical accuracy—The positional accuracy of a data set with respect to a specified vertical datum.

Coordinates—A set of N numbers designating the location of a point in N-dimensional space. Horizontal coordinates are two-dimensional coordinates, normally expressed as x, y coordinates, eastings, and northings, or longitude and latitude (geographic coordinates).

Crustal deformation—The deformation of the Earth's crust in response to stress.

Datum—A set of constants specifying the coordinate system used for geodetic control (i.e., for calculating coordinates of points on the Earth).

Horizontal datum (geometric reference frame)—A geodetic datum specifying the coordinate system in which horizontal control points are located. TUREF is the official horizontal datum of Turkey.

Vertical datum—A set of constants defining a height (elevation) system containing a coordinate system and points that have been consistently determined by observations, corrections, and computations. Turkish Vertical Control Network - 1999 (TUDKA99) is the official vertical datum of Turkey.

Calibration—In measurement technology, calibration is the comparison of measurement values delivered by a device under test with those of a calibration standard of known accuracy. Such a standard could be another measurement device of known accuracy, a device generating the quantity to be measured such as a heat, a sound tone, or a physical artifact, such as a meter ruler.

Epoch—A moment in time used as a reference for a model that has time dependence.

Geodesy—The science of accurately measuring and understanding the Earth's geometric shape, its orientation in space, its gravity field, and changes in these properties over time.

Geodetic control network—(also geodetic network, reference network, control point network, or control network) is a network, which is measured precisely by techniques of terrestrial surveying (e.g. precise levelling) or by satellite geodesy. A geodetic control network consists of stable, identifiable points, marked and monumented on the crust, with published datum values derived from observations that tie the points together.

Geodynamics—The study of Earth's internal forces (dynamics) and their impacts. Geodynamics is generally concerned with processes that move materials throughout the Earth. In the Earth's interior, movement happens when rocks melt or deform and flow in response to a stress field. This deformation may be brittle, elastic, or plastic, depending on the magnitude of the stress and the material's physical properties, especially the stress relaxation time scale. Experts in geodynamics commonly use data from geodetic GPS, InSAR, and seismology, along with numerical models, to study crustal deformations.

Global Navigational Satellite System (GNSS)—General term for satellite-based positioning systems like GPS, GLONASS, Galileo, and COMPASS.

Global Positioning System (GPS)—A satellite-based navigation and positioning system that enables horizontal and vertical positions to be determined; a global navigation satellite system (GNSS) maintained and operated by the United States.

International Earth Rotation Service (IERS)—Serves the astronomical, geodetic, and geophysical communities by providing data and standards related to Earth rotation and reference frames.

International GNSS Service (IGS)—An international service under the International Association of Geodesy (IAG) for coordinating analysis and distribution of GNSS data and data products.

International Terrestrial Reference System (ITRS)—describes procedures for creating reference frames suitable for use with measurements on or near the Earth's surface. The ITRS defines a geocentric system of coordinates.

International Terrestrial Reference Frame (ITRF)—is a realization of the ITRS. Its origin is at the center of mass of the whole earth including the oceans and atmosphere. New ITRF solutions are produced

every few years, using the latest mathematical and surveying techniques to attempt to realize the ITRS as precisely as possible. The most accurate global reference frame for scientific and other applications.

Monitoring—Geodetic methods are used to measure the movement of the Earth's surface and strain in the upper part of the Earth's crust. Repeated or continuous geodetic measurements have applications for the determination of horizontal and vertical displacements with time and research into underlying physical processes

Monumentation—The practice of marking known horizontal, vertical, gravity, or other control points with permanent structures, such as concrete/steel pillars and metal plaques. Once surveyed and marked, these monuments can be used for further surveying and infrastructure. Good monumentation for a geodetic observing site is where the antenna mounting is durable and stable, the site environment has minimal impact on the measurement signal, and the location of the reference point for each instrument can be precisely determined

Reference frame—A set of three-dimensional Cartesian coordinates (x, y, z), and the rates of change of these coordinates over time, for a network of points on the Earth's surface that defines the coordinates for other sites.

Reference system—The theories, models, and physical constants underlying a reference frame.

Precision—A measure of the repeatability of a measurement. Precision quantifies the ability to repeat the determination of a position within a reference frame (internal precision) and can be measured using various statistical methods on samples of estimated positions. Although precision does not imply accuracy, high precision is a prerequisite for consistently high accuracy and is necessary to resolve changes in position over time.

Time series—is a series of a component of coordinates indexed (or listed or graphed) in time order. Most commonly, a time series is a sequence taken at successive equally spaced points in time. Thus, it is a sequence of discrete-time data. Examples of time series in our project are heights of stations or horizontal coordinates.

Time series analysis—comprises methods for analyzing time series data to extract meaningful statistics and other characteristics of the data.

4. INTRODUCTION

The project “Development of Palestinian National Geodetic Reference Framework (PAL-GRF)” is a sub-component (2.2) of the “West Bank & Gaza Real Estate Registration Project (RERP)”, which is being carried out with the financial support of the World Bank.

PAL-GRF is implemented under the responsibility of Palestine Land Authority (PLA), the national agency responsible for property registration and related transactions, including transfers and mortgages, and state property management.

Geodetic Infrastructure constitutes the main base for all kind of position related technical works. It is essential to establish a modern and countrywide geodetic infrastructure for the production of modern and up-to-date cadastral and topographical maps.

A consistent and accurate geodetic control enables to systematically register all spatial information to allow their integration into map production, Land Information Systems, Cadastral works, Geographic Information Systems (GIS) and other projects that use geospatial data. Geodetic data, the product of geodetic control, are essential to the development of GIS and serve as one of the primary components of the National Spatial Data Infrastructure (NSDI).

The Palestinian geodetic reference system, as in the whole world, was initially established using classical surveying techniques, but it has not yet been integrated with global geodetic reference systems in the modern sense. The triangulation network and the height network were established by the Survey Department of Palestine about 100 years ago.

These networks are far from meeting today's expected accuracy criteria and modern positioning needs for various reasons such as low position accuracy and destruction of a significant part of the points. This issue was raised by the working group on geodesy (State of Palestine Country Report, August 2020) that “all available geodetic networks in Palestine are outdated, inconsistent, cause significant errors, and are not regulated”. Another important factor is the effect of crustal deformation that change the position of the points over time in the region where Palestine is located.

Currently, geodetic point positioning is based on Continuously Operating Reference Stations (CORS) operated by private sector and using the correction data provided by them. It cannot be said that there is a standard and homogeneous approach to the country level.

The modernization of reference frame is aimed at addressing the problem of using an outdated reference for surveying and mapping despite its changes. Today, modern geodetic infrastructure is basically designed to provide accurate, reliable and fast geospatial data to meet specified accuracy standards of 3-D coordinates (including physical heights) and their variations over time.

According to the analysis of the existing Palestine geodetic infrastructure in the scope of the tasks, methodology and the technology; it has been decided to establish a modern geodetic infrastructure that allows positioning for all user community with all aspects.

Geodetic positioning is the determination of the geometrical coordinates with respect to the Earth’s geometry, and physical heights with respect to the Earth’s gravitational potential field. Positioning tasks should be referenced to a national Palestine Geodetic Reference Frame (PAL-GRF). PAL-GRF will be defined with respect to the International Terrestrial Reference Frame (ITRF), which is endorsed by the IUGG. The PAL-GRF will provide this common geodetic positional system, the foundation for using geospatially referenced data and cost-effective sharing of governmental data resources, to form the digital framework of the NSDI.

5. OBJECTIVES, TASKS AND SCOPE OF THE WORK

In the modern sense, the new reference frame (PAL-GRF) will be a network of points having four-dimensional positions that are monumented and maintained for reliability and ease of use and the relation to the national and international frames will be realized.

The Palestine Geodetic Reference Frame (PAL-GRF) will be established by the GNSS data observed at selected stations.

IAG, in 2019 General Assembly in Canada "*resolved to recommend to the user community that the ITRF be the standard terrestrial reference frame for positioning, satellite navigation and Earth science applications, as well as for the definition and alignment of national and regional reference frames*".

In accordance with the IUGG-IAG resolutions above, the (PAL-GRF) will be defined in a geodetic datum of the International Terrestrial Reference Frame (ITRF).

The realization of the (PAL-GRF) will be carried out by the combined adjustment of GNSS data from surrounding International GNSS Service (IGS) permanent stations. The IGS final products (satellite ephemerides, earth rotation parameters, satellite clock parameters, differential code biases etc.) will be used in the post processing of GNSS data. The set of station coordinates in latest ITRF of the IGS stations will be held as the fiducial points in the network adjustment. Thus, a set of coordinates (X, Y, Z) and latitude and longitude and height, based on ITRF (geodetic horizontal and vertical datum) will be available for the components of PAL-GRF. Then, PAL-GRF will be integrated with the international community. The PAL-GRF will be the Palestine realization of the International Terrestrial Reference System.

General work plan of the project is given in Table 5-1. This report mainly covers the items D-3, D-4, D-5, D-6 and D-8.

PLA, first selected 10 PAL-GRF stations and then conducted four measurement campaigns. The Consultant pre-processed the GNSS data and confirmed the status of the data for the suitability for being a network station.

Then, four campaign GNSS data, with the addition of GNSS data from selected fiducial IGS stations, were post-processed by the Consultant with Bernese GNSS Software. Finally, the set of stations coordinates in ITRF2020 (2023.50) has been produced for further use.

Below is the report for the part of the establishment of the PAL-GRF.

Table 5-1: Work plan of the establishment of PAL-GRF

N°	Deliverables	Duration (Month)	Date (Month) for delivery
D-1	Project Implementation Plan for PAL-GRF	1	T0 + 1
	1) Project technical specifications	1	T0 + 1
	2) Geodetic Control Network design	1	T0 + 1
	Client's Approval (*)	1	T0 + 2
D-2	Specifications and tender documents for the field survey works & data acquisition.	2	T0 + 3
	Tender process for selecting a qualified geodetic surveying contractor (*)	2	T0 + 5
D-3	Site selection and Field survey, Preliminary Survey Reports & Testing report including the signal quality and data flow stability.	2	T0 + 7
D-4	Review and acceptance of Observation files & raw data provided by the Surveying Company.	2	T0 + 8
D-5	Review and acceptance of the preliminary and final survey	2	T0 + 8
	1) Preliminary Survey	1	T0 + 6
	2) Final survey	1	T0 + 8
D-6	Final Coordinate list in PAL-GRF and Old System (Palestine Grid 1923)	2	T0 + 9
	1) Post Processing of GNSS data	1	T0 + 8
	2) PAL-GRF definition wrt the latest ITRF	2	T0 + 9
	Client's Approval (*)	2	
D-7	Technical specifications/TOR for the establishment of the Operational and Analysis Centers, including hardware and software	2	T0 + 11
D-8	Transformation parameters between Palestine Grid 1923 and the PAL-GRF	3	T0 + 11
D-9	Knowledge transfer, training and capacity building for 10 PLA staff (2 times for two weeks)	0.5	T0 + 4, T0 + 12
D	Final report	2	T0 + 12

6. DESCRIPTION OF THE SELECTED NETWORK STATIONS

6.1. PAL-GRF stations

PAL-GRF stations were selected by the PLA staff on the field. 10 stations, which are candidate for -future CORS network stations, were selected and observed within the PAL-GRF establishment works.

The PAL-GRF stations are depicted on the Figure 6-1 below.

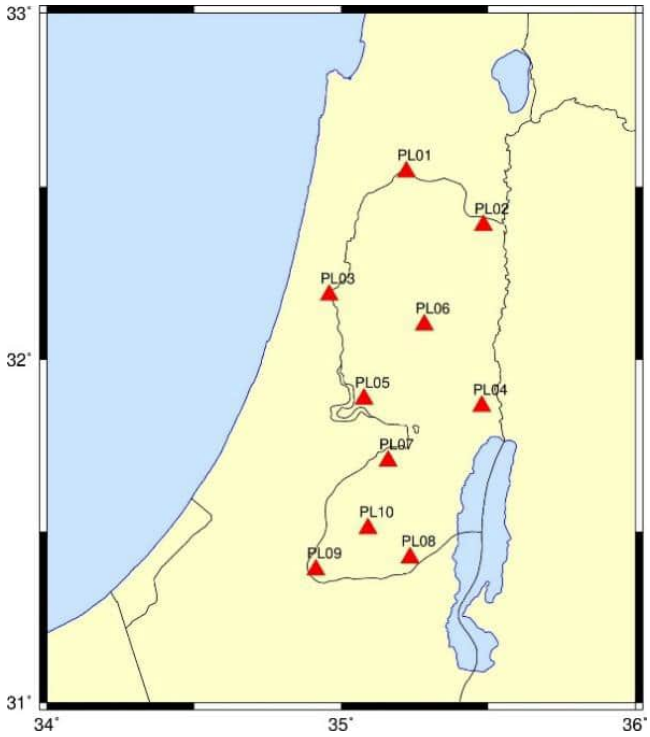

Figure 6-1: PAL-GRF stations

The PAL-GRF stations were selected in the west bank area considering logistics, security, etc. All of the stations are monumented with a steel pillar having forced centering holes. The consultant supplied the material and the PLA staff constructed the pillars. Sample photographs of the network stations are given in Figure 6-2.

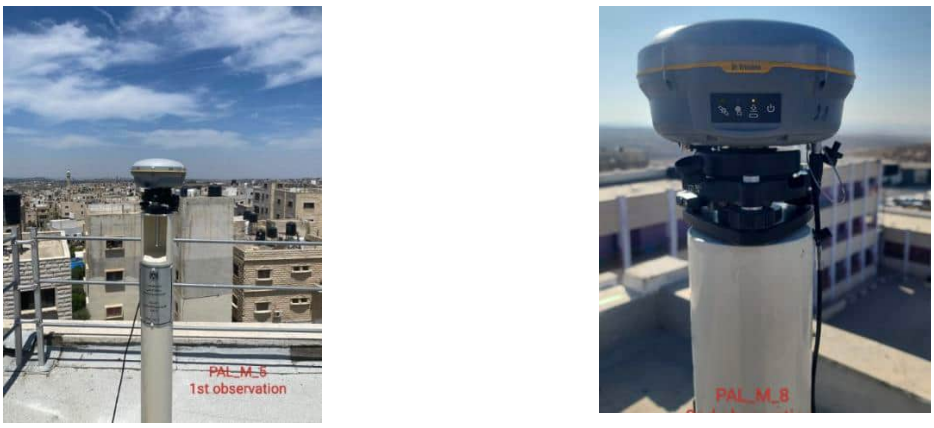

Figure 6-2: Sample photographs of selected PAL-GRF stations

6.2. IGS stations

There are a number of IGS stations around the territory of Palestine, except the south direction. First, we examined the time series of station coordinates in order to select the ones which are stable with time and the ones with precise coordinates and associated velocities defined in ITRF2020. Enough number of the stations must be selected in order to make sure that the PAL-GRF can be very well compatible with ITRF2020

Moreover, we selected 14 IGS/ITRF stations around the territory of Palestine. The IGS/ITRF stations are shown in Figure 6-3.

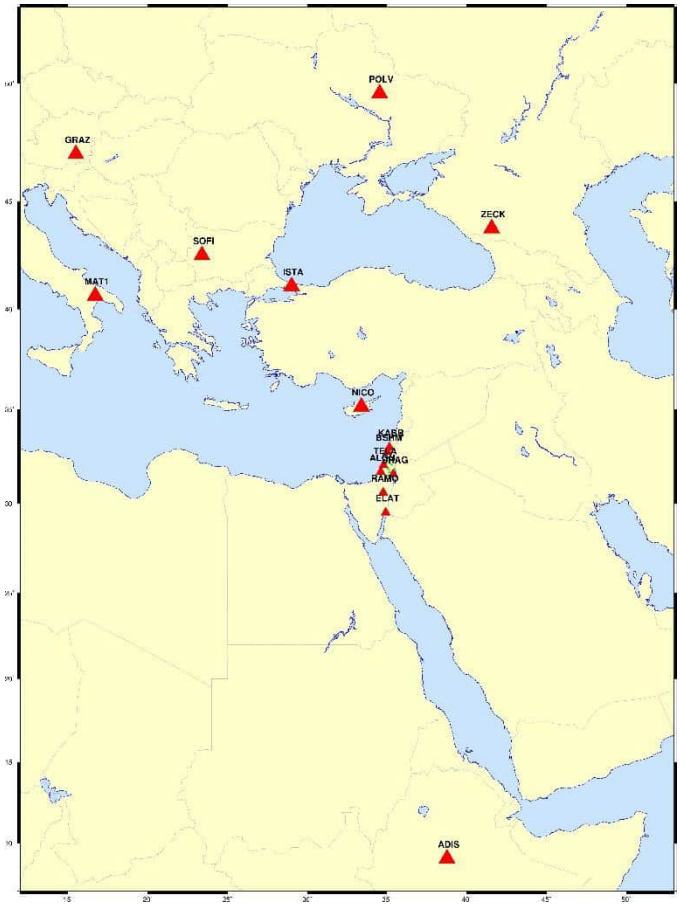

Figure 6-3: IGS and ITRF stations selected for the establishment of PAL-GRF.

6.3. Fiducial ITRF stations

One of the main constraints of the new PAL-GRF is to determine the coordinates in ITRF2020. For this reason, we need to add some more fiducial stations to be introduced to the processing with their ITRF coordinates and associated velocity field. The International GNSS Service (IGS) has been operating a number of continuously observing permanent GNSS stations distributed globally. Besides, IGS also takes GNSS data from some other GNSS stations, which are operated by different national institutions, into the processing, and thus computes and releases the coordinates of all stations in ITRF for public use. The GNSS data observed at those stations are also publicly available.

On the other hand, the distribution of the IGS stations with respect to Palestine is not so good, since there are a few stations on the continent of Africa. This constrains us to select more fiducial stations in the vicinity of Palestine, and thus we selected some nearby stations included in the ITRF2020 solution, to be used in the establishment of PAL-GRF with their data, coordinates and velocity field. We selected 3 ITRF2020 stations (ALON, ELAT and TELA) additionally. So, the final picture around the local network is given in Figure 6-3.

6.4. Set of station coordinates and velocities

The PAL-GRF were defined in the latest realization of the ITRF, namely the ITRF2020. The coordinates and velocities of the selected IGS and ITRF stations in ITRF2020 at epoch 2015.0 are given in Table 6-1 below.

Table 6-1: Cartesian coordinates of stations in ITRF2020 (2015.0)

NAME	X (m)	Y (m)	Z (m)	v_X (mm/y)	v_Y (mm/y)	v_Z (mm/y)	Tectonic Plate	Network
ADIS	4913652.7609	3945922.6696	995383.3331	-0.01922	0.01671	0.01820	AFRC	IGS
BSHM	4395951.1833	3080707.2289	3433498.2609	-0.02128	0.01243	0.01670	AFRC	IGS
DRAG	4432980.6621	3149432.0930	3322110.4410	-0.01986	0.01423	0.01873	AFRC	IGS
GRAZ	4194424.1240	1162702.4605	4647245.1930	-0.01695	0.01798	0.01039	EURA	IGS
ISTA	4208830.7260	2334850.0235	4171267.0890	-0.01773	0.01609	0.01002	EURA	IGS
NICO	4359415.5352	2874117.1781	3650777.9518	-0.01817	0.01118	0.01257	EURA	IGS
MAT1	4641951.2685	1393053.8493	4133281.0073	-0.01858	0.01903	0.01460	EURA	IGS
POLV	3411557.3382	2348463.8352	4834396.6426	-0.01998	0.01340	0.00833	EURA	IGS
RAMO	4514721.8549	3133507.8433	3228024.6792	-0.02100	0.01411	0.01705	ARAB	IGS
SOFI	4319372.3900	1868687.5700	4292063.8000	-0.01698	0.01874	0.00827	EURA	IGS
ZECK	3451175.6956	3060336.4325	4391958.8536	-0.02210	0.01427	0.00890	EURA	IGS
ALON	4470258.1511	3084589.7721	3332952.7759	-0.02060	0.01326	0.01676	AFRC	ITRF2020
ELAT	4555028.6509	3180067.3419	3123164.4310	-0.02194	0.01602	0.01847	ARAB	ITRF2020
TELA	4443535.3843	3086140.8911	3366854.2050	-0.02068	0.01357	0.01749	ARAB	ITRF2020

6.5. Frame Definition of the ITRF2020

6.5.1. Origin

The origin of the ITRF2020 long-term frame is defined in such a way that there are zero translation parameters at epoch 2015.0 and zero translation rates between the ITRF2020 and the ILRS SLR long-term frame over the time-span 1993.0-2021.0, using the concept of internal constraints.

The origin of the ITRF2020 seasonal signals expressed in the CM (as sensed by SLR) frame is defined in such a way that there is no seasonal translation between the ITRF2020 seasonal signals and the input SLR solutions over the time-span 1993.0-2021.0, using the concept of internal constraints.

The origin of the ITRF2020 seasonal signals expressed in the CF frame is defined in such a way that the weighted sum of the seasonal signals of a selected subset of stations (approximating an integral over the Earth's surface) is zero.

6.5.2. Scale

The scale of the ITRF2020 long-term frame is determined using internal constraints, in such a way that there are zero scale and scale rate between ITRF2020 and the scale and scale rate averages of VLBI selected sessions up to 2013.75 and SLR weekly solutions covering the time-span 1997.7 – 2021.0.

The scale of the ITRF2020 seasonal signals, expressed in both the CM and CF frames, is determined using internal constraints, in such a way that the average of the seasonal scale variations between the selected SLR solutions and ITRF2020 is zero.

6.5.3. Orientation

The orientation of the ITRF2020 long-term frame is defined in such a way that there are zero rotation parameters at epoch 2015.0 and zero rotation rates between the ITRF2020 and ITRF2014. These two conditions are applied over a core network.

The orientation of the ITRF2020 seasonal signals, expressed in both the CM and CF frames, is defined in such a way that there is no net seasonal rotation of that same core network.

7. GNSS OBSERVATIONS AT PAL-GRF STATIONS

7.1. Method of GNSS measurements in PAL-GRF network

PAL-GRF network consists of 10 local stations and all the GNSS observations were carried out by the PLA staff. All the network stations are monumented with steel pillars having forced centering.

PAL-GRF stations were observed three/four times as given in Table 7-1 and Table 7-2. Each observation session lasted at least 8 hours with 1/10/30 sec data intervals. However, we used 30 second data interval same as IGS does. All of the GNSS observations were converted to RINEX format for further computations. The receivers, antennas and other observation parameters are given in Table 7-2 below. The observation log sheets, prepared at the field by the PLA staff, are given in Appendix-A.

Table 7-1: GNSS observations collected at PAL-GRF stations

Session	Date	Day of the year (doy)	GPS week_day
1	07.06.2023	158	2265_3
2	03.07.2023	184	2269_1
3	17.07.2023	198	2271_1
4	26.07.2023	207	2272_3

Table 7-2: GNSS observation parameters

St.	Date	Start Time	End Time	Receiver		Antenna		Ant. Hgt.
PL01	2023-07-03	05:31:30	17:37:00	TRIMBLE	R8S	TRMR8S	NONE	0.154
PL01	2023-07-17	05:26:00	17:45:00	TRIMBLE	R8S	TRMR8S	NONE	0.150
PL02	2023-06-07	05:18:00	17:46:00	TRIMBLE	R8S	TRMR8S	NONE	0.155
PL02	2023-07-03	05:23:30	17:33:00	TRIMBLE	R8S	TRMR8S	NONE	0.158
PL02	2023-07-17	04:59:00	17:30:30	TRIMBLE	R8S	TRMR8S	NONE	0.153
PL03	2023-06-07	05:18:00	17:46:00	TRIMBLE	R8S	TRMR8S	NONE	0.155
PL03	2023-07-03	05:23:30	17:33:00	TRIMBLE	R8S	TRMR8S	NONE	0.158
PL03	2023-07-17	04:59:00	17:30:30	TRIMBLE	R8S	TRMR8S	NONE	0.153
PL04	2023-06-07	05:18:00	17:46:00	TRIMBLE	R8S	TRMR8S	NONE	0.155
PL04	2023-07-03	05:23:30	17:33:00	TRIMBLE	R8S	TRMR8S	NONE	0.158
PL04	2023-07-17	04:59:00	17:30:30	TRIMBLE	R8S	TRMR8S	NONE	0.153
PL04	2023-07-26	05:24:00	17:50:30	TRIMBLE	R8S	TRMR8S	NONE	0.157
PL05	2023-06-07	05:40:30	18:00:00	TRIMBLE	R8S	TRMR8S	NONE	0.085
PL05	2023-07-03	04:33:30	17:48:00	TRIMBLE	R8S	TRMR8S	NONE	0.158

PL05	2023-07-17	06:14:00	17:40:00	TRIMBLE	R8S	TRMR8S	NONE	0.155
PL05	2023-07-26	05:03:30	17:52:00	TRIMBLE	R8S	TRMR8S	NONE	0.151
PL06	2023-06-07	05:18:00	17:46:00	TRIMBLE	R8S	TRMR8S	NONE	0.155
PL06	2023-07-03	05:23:30	17:33:00	TRIMBLE	R8S	TRMR8S	NONE	0.158
PL06	2023-07-17	04:59:00	17:30:30	TRIMBLE	R8S	TRMR8S	NONE	0.153
PL07	2023-06-07	05:18:00	17:46:00	TRIMBLE	R8S	TRMR8S	NONE	0.155
PL07	2023-07-03	05:23:30	17:33:00	TRIMBLE	R8S	TRMR8S	NONE	0.158
PL07	2023-07-17	04:59:00	17:30:30	TRIMBLE	R8S	TRMR8S	NONE	0.153
PL07	2023-07-26	05:46:30	17:50:30	TRIMBLE	R8S	TRMR8S	NONE	0.155
PL08	2023-06-07	05:25:30	18:00:30	TRIMBLE	R8S	TRMR8S	NONE	0.156
PL08	2023-07-03	05:12:00	17:36:30	TRIMBLE	R8S	TRMR8S	NONE	0.155
PL08	2023-07-17	05:35:30	17:31:00	TRIMBLE	R8S	TRMR8S	NONE	0.154
PL09	2023-06-07	05:58:30	18:00:00	TRIMBLE	R8S	TRMR8S	NONE	0.153
PL09	2023-07-03	05:12:00	17:36:30	TRIMBLE	R8S	TRMR8S	NONE	0.084
PL09	2023-07-17	04:44:30	17:43:30	TRIMBLE	R8S	TRMR8S	NONE	0.151
PL09	2023-07-26	05:38:00	18:24:30	TRIMBLE	R8S	TRMR8S	NONE	0.153
PL10	2023-06-07	05:29:30	18:00:30	TRIMBLE	R8S	TRMR8-4	NONE	0.155
PL10	2023-07-03	06:01:00	17:36:30	TRIMBLE	R8S	TRMR8-4	NONE	0.157
PL10	2023-07-17	05:48:00	17:31:00	TRIMBLE	R8S	TRMR8-4	NONE	0.155
PL10	2023-07-26	05:38:00	17:55:00	TRIMBLE	R8S	TRMR8-4	NONE	0.155

Antenna height measurement is essential in GNSS observations. Antenna height must be given with respect to the Antenna Reference Point (ARP) of the antenna. ARP of the Trimble antennas used in this work are given below Figure 7-1. All of the antenna height measurements recorded in the field are converted to ARP antenna height with respect to the figures given.

Figure 7-1 originally were given in file “https://files.igs.org/pub/station/general/antenna.gra”.

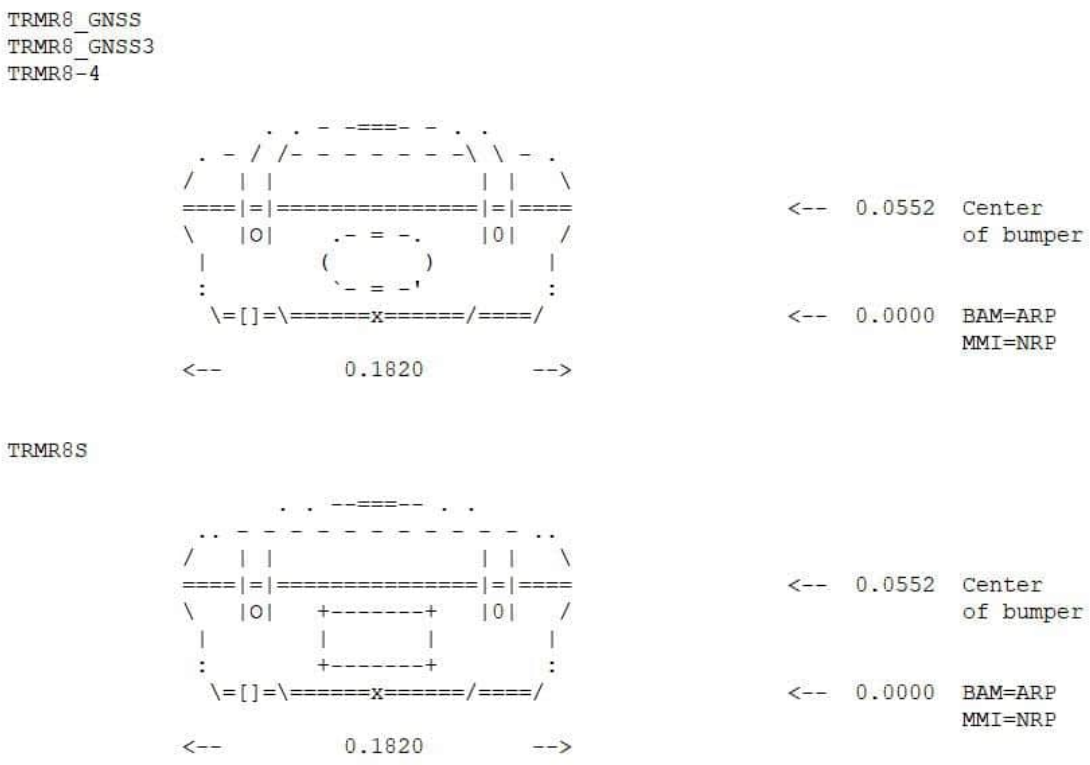

Figure 7-1: Antenna Reference Point of the Trimble R8-4 and R8S Antenna (antenna.gra)

7.2. Quality check of the observations

A team of PLA selected and monumented all the PAL-GRF stations. Then, PLA staff run a test measurement session (doy 158) to assess the site conditions for GNSS signal reception. The data and conclusions for this site test need to be reported to PLA with the Contractor liability acceptance for the site selected or its rejection as a result of the tests conducted. The data have been analyzed by the Consultant using TEQC software, which is released by UNAVCO (www.unavco.org), in order to ensure the quality. TEQC is a comprehensive toolkit for solving many problems when preprocessing GNSS data:

- translation: read GNSS native receiver files and translate the data to other formats
- editing: metadata extraction, editing, and/or correction of RINEX header metadata or BINEX metadata records; as well as cutting/splicing of RINEX files or BINEX files
- quality checking of GPS and/or GLONASS data (native binary, BINEX, or RINEX observation files, with or without navigation files with ephemerides)

The three functions from which *teqc* gets its name, translation, editing, and quality checking, can be performed separately, in pairs, or all together in a single run. TEQC uses a command line interface, speeding execution of routine or repeated processing, allowing use of TEQC in scripts, and avoiding the repetitive menu clicking required by a graphical user interface.

We processed the GNSS data from doys_158-184-198-207 with the TEQC software.

The output summary file is the '`PL011980.23S`' in the same directory, which are produced for all observation files that are quality checked.

The overall summary of the quality check of all files (*.23S) are given in Appendix-B and the summary lines are given in Table 7-3.

Table 7-3: summary of the quality check of all files

Summary NAMEddds	date			Start time	End time	Duration (hr)	dT	#expt	#have	%	mp1 (cm)	mp2 (cm)	Ratio o/slps
PL011580.23S	23	6	7	05:43	16:30	10.80	10	60317	57849	96	42	25	2410
PL011840.23S	23	7	3	05:31	17:37	12.10	10	70172	64233	92	44	27	12847
PL011980.23S	23	7	17	05:25	17:45	12.33	10	69703	63233	91	45	29	1193
PL021580.23S	23	6	7	05:18	17:46	12.48	10	70400	67049	95	57	35	5158
PL021840.23S	23	7	3	05:23	17:35	12.18	10	70781	64682	91	59	38	32341
PL021980.23S	23	7	17	04:59	17:30	12.53	10	70987	62760	88	65	42	747
PL031580.23S	23	7	3	06:01	17:38	11.62	10	66166	58187	88	47	35	1662
PL031840.23S	23	7	3	05:33	17:36	12.05	10	69601	63516	91	46	38	63516
PL031980.23S	23	7	17	05:16	17:24	12.13	10	68650	63392	92	48	38	10565
PL041580.23S	23	6	7	09:46	17:57	8.18	10	45109	42411	94	47	30	10603
PL041840.23S	23	7	3	05:08	17:36	12.40	10	72102	65748	91	49	32	65748
PL041980.23S	23	7	17	05:33	17:30	11.95	10	67065	61149	91	52	35	1911
PL042070.23S	23	7	26	05:23	17:50	12.45	10	70047	64003	91	49	33	64003
PL051580.23S	23	6	7	05:40	18:00	12.34	10	70224	67672	96	40	27	67672
PL051840.23S	23	7	3	04:33	17:48	13.25	10	76094	70173	92	39	29	11696
PL051980.23S	23	7	17	06:13	17:40	11.44	10	63959	58893	92	43	26	58893
PL052070.23S	23	7	26	05:03	17:52	12.82	10	71928	65962	92	43	26	65962
PL061580.23S	23	6	7	05:30	13:36	8.09	10	45406	44382	98	43	24	44382
PL061840.23S	23	7	3	04:57	17:33	12.59	10	72848	66895	92	45	26	66895
PL061980.23S	23	7	17	05:32	17:30	11.98	10	67089	60928	91	46	28	1741
PL071580.23S	23	6	7	05:50	18:25	12.57	10	72413	69226	96	43	26	69226
PL071840.23S	23	7	3	05:14	17:57	12.72	10	72736	66806	92	43	27	22269
PL071980.23S	23	7	17	05:50	17:37	11.79	10	65930	60705	92	45	26	60705
PL072070.23S	23	7	26	05:46	17:50	12.07	10	67670	61776	91	45	29	5148
PL081580.23S	23	6	7	05:25	18:00	12.60	15	47801	45804	96	83	50	1018
PL081840.23S	23	7	3	05:12	17:36	12.41	10	71122	65167	92	81	44	1862
PL081980.23S	23	7	17	05:31	17:31	11.93	10	67381	61889	92	76	43	2134
PL091580.23S	23	6	7	05:58	18:00	12.03	10	68510	65871	96	50	30	32936
PL091840.23S	23	7	3	05:10	17:37	12.45	10	71378	65399	92	46	34	21800
PL091982.23S	23	7	17	04:43	17:43	13.00	10	72916	67674	93	51	32	4834
PL092070.23S	23	7	26	05:37	18:24	12.79	10	71514	65047	91	52	34	4646
PL101580.23S	23	6	7	05:28	18:03	12.57	15	47325	44006	93	48	34	1073
PL101840.23S	23	7	3	06:01	17:38	11.62	10	66166	58187	88	47	35	1662
PL101980.23S	23	7	17	05:47	17:40	11.88	10	66407	59029	89	51	35	1093
PL102070.23S	23	7	26	05:28	17:55	12.44	10	69498	60870	88	50	34	1171

The summary line shows the start and end times of the window (time format is year month day hour min), the length of the time window in hours (hrs), the observation interval in seconds (dt), the number of possible observations (#expt) above the elevation mask, the number of complete observations (#have), the ratio of complete to possible observations as a percent (%), the rms “multipath combinations” values mp1 and mp2, and lastly the "observations per slip" (o/slps). We have obtained the 92% of the expected observations. The computed values for mp1 and mp2 vary between 39-83 cm and 24-50 cm respectively.

The ‘mp’ values on the summary lines are rounded to the nearest centimeter. "Observations per slip" (o/slps) combines "observations" meaning "complete observations" (above the elevation mask), with the number of “slips.” One "slip" means either an ionosphere delay observation slip and/or both mp1 and mp2 slips occurred during an epoch having a complete observation for the specific SV. The value ‘o/slps’ is the ratio, typically a few hundred or more. This value varies between 747 and 69226 in our work.

The summary of the *teqc* execution evidently shows that all the GNSS data collected at PAL-GRF stations are in good condition and quality to be used in further processing. All of the data set is pre-processed in order to check/edit/confirm the metadata within the Rinex files. The first column in Table 7-3 shows the *rinex* data files as well as other meta data.

8. POST-PROCESSING OF THE GNSS DATA

All GNSS data collected at PAL-GRF stations have been be post-processed by using Bernese GNSS software as given below.

Continuous GNSS data from IGS stations were downloaded from IGS data centers. All the GNSS data collected at PAL-GRF stations and IGS/ITRF stations are given in Appendix-C and Appendix-D respectively.

IGS analysis centers process the IGS data on a daily basis and produces the best possible consistent GPS and GLONASS satellite orbits and the other products (see Appendix-E).

Every day, precise satellite orbits and station coordinates, earth rotation parameters, satellite and receiver clock corrections, global ionosphere maps and station troposphere parameters are computed and made available for geodetic and surveying applications. They contribute, e.g., to the monitoring and maintenance of the International Terrestrial Reference Frame (ITRF). IGS final orbits are usually available on the thirteenth day after the last observation and includes both GPS and GLONASS satellite orbit information (https://cddis.gsfc.nasa.gov/archive/gnss/products/).

We use Bernese Software V5.2 for GNSS post processing, which is formally used at CODE as standard tool. Due to the use of same software, we deemed appropriate to adopt the similar strategy followed by CODE and to use all of its product in order to provide consistency. The details of the processing are given in Bernese Manual, which is available at www.bernese.unibe.ch/docs/DOCU52.pdf.

Therefore, we have processed the PAL-GRF GNSS data using the standard strategy.

8.1. Processing strategy for the GNSS Data

Local PAL-GRF GNSS data are processed by adding data from IGS/ITRF stations around the region. The first step of the processing is to create a campaign and related directory structure. Once the campaign is created the related directories are also created within Bernese user menu.

All the data within the same day are considered as a session. Processing was carried out in session mode. First of all, RINEX data were converted to Bernese observation file format. All Bernese observation files (*.CZH, *.CZO, *.PZH, *.PZO) are stored in OBS directory of the campaign.

Then, the Earth Rotation Parameters (*.iep) obtained from IGS/CODE are converted to Bernese format so as to produce daily Bernese *.erp files to be used in processing.

The IGS/CODE standard product of precise orbits (*.pre) are produced in daily basis within the specific GPS week. All the necessary .pre files were downloaded and then converted into Bernese orbit format. Bernese specific orbit files (*.ERP, *.TAB and *.STD) are stored in ORB directory. Moreover, ionosphere files (*.ION), differential code biases files (*.DCB) and number of input files were also downloaded and stored in related directories.

Parameter estimation in the Bernese GNSS Software is based on Least-Squares Estimation (LSE). The two main programs in the software package allowing for the adjustment of model parameters to GNSS observations are GPSEST and ADDNEQ2.

GPSEST processes the observations. It sets up the observation equations and solves the normal equation (NEQ) while ADDNEQ2 manipulates and combines solutions on the normal equation level. GPSEST offers many processing options. Additional options are available in program ADDNEQ2 such as datum definition by means of free network condition, writing of coordinate SINEX file, or estimation of station velocities.

All the parameters are computed and normal equation system is stored in GPSEST run. Actually, we form the loosely constrained (LC) normal equation systems (NEQs) with GPSEST. All the sessions were processed with GPSEST and LC NEQs (R1*.NEQ) for each day was formed and stored in SOL directory.

Then we may define the geodetic datum and combine all LC NEQs with ADDNEQ2 module of the Bernese software. The program ADDNEQ2 was developed to compute multi-session solutions from the combination of a set of single-session solutions. GPSEST is in general used to process individual sessions while combination of different sessions is done with ADDNEQ2.

8.2. Combination of the Daily Solutions and Datum Definition

All the data collected in each day (session) were post-processed and daily loosely constrained (free) normal equation systems are obtained. All daily normal equation system files are given in Appendix-F. Once the daily free solutions are obtained from GPSEST program, then it may be possible to combine them with a suitable geodetic datum definition so as to compute the repeatability and coordinates of the network stations. Combination of loosely constrained daily solutions is carried out by making use of ADDNEQ2 program of the Bernese GNSS Software.

The mathematical model for the combination and solution of the free NEQs is given in Bernese Manual in detail. In the combination process some additional parameters may be introduced, the most important of which is the linear velocity of the coordinate components of the stations.

As having more than one LC NEQ, they may be solved either sequentially or in a common adjustment. The result of a Least Squares Estimation (LSE) using all observations in one step is the same as when splitting up the LSE in different parts and combining the results later as long as these parts are independent. The identity of both methods has been proved in (Bernese V5.2 documentation).

Normal equations can be manipulated in different ways;

- normal equation scaling
- expansion of normal equations
- transformation of parameters
- transformation of a priori parameter information
- stacking of parameters
- reduction of parameters
- introduction of additional parameters
- parameter elimination
- parameter constraining

The daily loosely constrained solutions are used for later computations. The daily solutions are combined to obtain epoch-wise loosely constrained campaign solution. By this way it is allowed the reference frame to be defined in a further step for the computation of multi-year solutions.

8.3. Method for Determining GNSS Network Stability

8.3.1. GNSS Daily Repeatability

Daily free solutions are combined with a suitable datum definition so as to compute the repeatability and coordinates of the network stations. Combination of loosely constrained daily solutions is carried out by making use of ADDNEQ2 program of the Bernese GNSS Software.

In order to check the consistency and quality of the daily solutions, a minimally constrained solution (No-Net-Translation) using fiducial stations is applied. Corrections to the published coordinates are examined to detect any misbehaving stations. Moreover, quality of the solutions is checked with the coordinate repeatability of the stations. The coordinates from the daily solutions are compared with the weighted average value and difference from the average value is calculated for each component (north, east and up) separately.

8.3.2. Stability Analysis of the Geodetic Datum of GNSS Network

The geodetic datum for all daily and combined solutions can be defined by applying minimum constraints using (No-Net-Translation) method on the coordinates of IGS stations in ITRF2020. Actually, 3 IGS fiducial stations are adequate for the geodetic datum definition in 3-D GNSS networks. In our project, we have used 14 fiducial stations in geodetic datum determination. The position and velocity information of the 14 IGS/ITRF stations have been obtained from the IGS server.

Minimum constraint solutions give information about the quality of the network and makes it possible to detect outlier observations. For daily and combined solutions where no velocity parameters introduced,

corrections to the published coordinates are examined to detect any misbehaving stations and datum defining stations. Moreover, quality of the solutions is checked with the coordinate repeatability of the stations. The coordinates from the daily solutions were compared with the weighted average value and difference from the average value is calculated for each component (north, east and up) separately.

In case any fiducial station shows different behavior from the others and corrections to its coordinates are considerably larger than the other stations, this station should be excluded from the datum definition for all solutions.

The very good agreement of the stations show with the published coordinates and velocities is an important indicator of the consistency of these points with respect to each other and stability of the GNSS network solutions.

9. RESULTS OF PAL-GRF GNSS MEASUREMENTS

This section covers the PAL-GRF 4-day GNSS measurement campaign and campaign based post-processing and adjustment results. Below are given the results of GNSS measurements carried out within the PAL-GRF. The results below are the supplementary information to the description of measurement methods and processing given in Section 8.

9.1. Summary of GNSS Observations

Table 9-1 shows the date of the observation, the day of the year and the observed stations. Table 9-2 shows the RINEX observation file list collected in the PAL-GRF campaign.

Table 9-1: Daily GNSS Observations Summary Record

Date	doy	Stations Observed									
07.06.2023	158	PL01	PL02	PL03	PL04	PL05	PL06	PL07	PL08	PL09	PL10
03.07.2023	184	PL01	PL02	PL03	PL04	PL05	PL06	PL07	PL08	PL09	PL10
17.07.2023	198	PL01	PL02	PL03	PL04	PL05	PL06	PL07	PL08	PL09	PL10
26.07.2023	207				PL04	PL05		PL07		PL09	PL10

Table 9-2: RINEX Observation File List collected in the PAL-GRF Campaign

PL011580.23O	PL041580.23O	PL061840.23O	PL091580.23O
PL011840.23O	PL041840.23O	PL061980.23O	PL091840.23O
PL011980.23O	PL041980.23O	PL071580.23O	PL091980.23O
PL021580.23O	PL042070.23O	PL071840.23O	PL092070.23O
PL021840.23O	PL051580.23O	PL071980.23O	PL101580.23O
PL021980.23O	PL051840.23O	PL072070.23O	PL101840.23O
PL031580.23O	PL051980.23O	PL081580.23O	PL101980.23O
PL031840.23O	PL052070.23O	PL081840.23O	PL102070.23O
PL031980.23O	PL061580.23O	PL081980.23O	

9.2. Accuracy Assessment of GNSS Observations

Accuracy assessment of GNSS measurements is calculated based on the differences of measurements and intrinsic convergence of measurement results. In order to check the consistency of the IGS stations and accuracy of the daily solutions, daily solutions with different datum definitions have been combined. Minimum constrained solution by introducing No-Net-Translation on all fiducial IGS/ITRF stations has been obtained. As it can be seen from Table 9-3, corrections to the published coordinates of IGS stations are generally at sub-cm level except ISTA station, which was removed from the fiducial stations due to its inconsistency. This result shows that PAL-GRF stations are in good agreement and consistent with the IGS reference frame.

Table 9-3: Corrections to Coordinates of Fiducial Stations in the PAL-GRF Solution (mm)

STATION	X	Y	Z	U	N	E	Remark
ADIS	6.7	-1.0	-6.6	3.5	-7.3	-4.9	
ALON	-5.2	-1.2	3.2	-2.5	5.4	2.0	
BSHM	-9.7	-1.1	3.5	-5.4	7.6	4.7	
DRAG	-5.7	0.3	1.9	-2.8	4.0	3.6	
ELAT	-3.5	-4.5	-3.0	-6.2	0.1	-1.7	
GRAZ	9.6	2.5	19.6	21.1	6.1	-0.1	
ISTA	-4.4	56.5	-29.3	-1.6	-37.6	51.4	Excluded
MAT1	3.2	3.4	-2.2	1.6	-4.3	2.3	
NICO	1.7	-2.8	-1.5	-1.0	-1.1	-3.2	
POLV	5.2	6.0	-0.3	4.8	-6.0	2.0	
RAMO	-2.6	2.1	-0.6	-1.2	-0.1	3.2	
SOFI	-0.5	-3.0	-6.5	-5.6	-3.7	-2.6	
TELA	-7.5	-3.5	1.2	-6.3	5.4	1.4	
ZECK	8.4	2.9	-8.7	-0.1	-12.0	-3.4	

Hence, minimum constrained solution of the network by introducing No–Net–Translation condition on IGS stations is used for daily repeatability analysis. Daily repeatabilities for PAL-GRF stations are given in Table 9-4 and in Appendix-H. Average rms for the north, east and up components are 2.1 mm, 3.1 mm and 5.7 mm respectively. Figure 9-1 shows the RMS of daily repeatability plot for the PAL-GRF campaign.

The adjustment results were examined on the basis of the quality of the observed data, station coordinates (accuracy and repeatability) and RMS of differences in coordinate components (north, east, height).

Table 9-4: Repeatability of Stations in the PAL-GRF Solution

Station	Number of occupations	Repeatability (mm)		
		North	East	Up
PL01	3	2.61	1.23	8.17
PL02	3	4.92	0.62	6.17
PL03	3	4.69	4.89	1.33
PL04	4	2.02	4.09	3.81
PL05	3	2.41	3.9	15.54
PL06	3	4.37	0.96	1.94
PL07	4	1.56	3.94	1.67
PL08	3	1.57	4.64	4.97
PL09	4	2.29	7.71	8.44
PL10	4	1.88	4.53	4.72
ADIS	4	2.37	1.45	10.20
ALON	4	1.27	2.03	3.91
BSHM	4	1.87	0.51	3.02
DRAG	4	0.74	0.80	1.29
ELAT	4	0.59	2.19	4.77
GRAZ	4	1.42	4.36	4.71
ISTA	4	0.89	1.51	7.86

Station	Number of occupations	Repeatability (mm)		
		North	East	Up
MAT1	4	0.70	1.47	6.66
NICO	4	0.23	2.00	3.11
POLV	4	0.93	1.63	5.09
RAMO	4	0.51	0.58	2.70
SOFI	4	3.22	1.96	4.00
TELA	4	0.56	0.92	1.99
ZECK	4	0.52	1.94	3.84
TOTAL	**90**	**2.09**	**3.06**	**5.72**

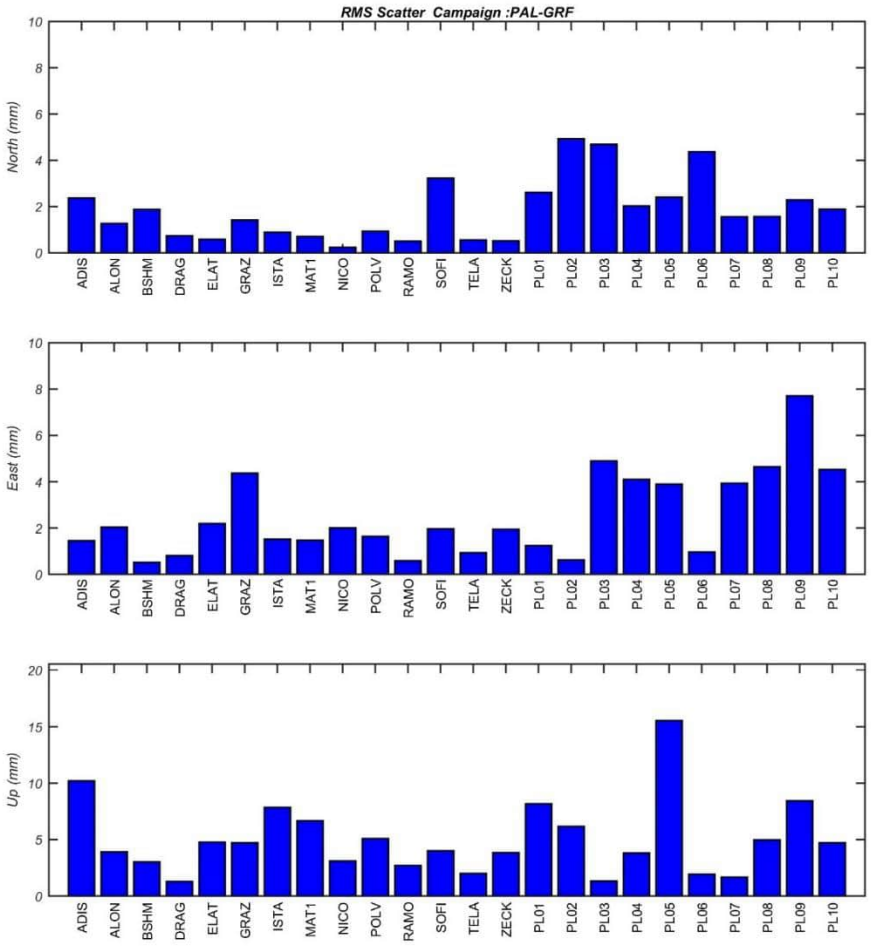

Figure 9-1: RMS of Daily Repeatability for the PAL-GRF Campaign

9.3. Adjustment of PAL-GRF GNSS Network

In the PAL-GRF campaign 10 GNSS stations were observed. In addition to the PAL-GRF stations RINEX data from IGS and ITRF2020 stations were obtained (see Appendix-C and Appendix-D). All the data were processed with CODE Analysis Center standard products by making use of Bernese GNSS Software (BSW52), and computed daily loosely constrained solutions.

Then, all daily loosely constrained solutions (Appendix-F) were combined with a suitable geodetic datum definition by using ADDNEQ2 program of Bernese Software. Finally, loosely constrained campaign solution and definitive coordinates of network stations were obtained in ITRF2020 (02.07.2023,

2023.50). The coordinates obtained from this minimally constrained solution (No-Net-Translation) based on fiducial IGS stations are given in Table 9-5 and Table 9-6. As it is well known, wherein coordinates, which may slightly vary depending on the datum definition, reflect the results of the specific campaign only. The results of the network adjustment are given in Appendix-G.

The so-called loosely constrained solutions will be used, in the future, for the combination of epoch wise solutions and estimation of the station coordinates as well as their associated velocity field. The loosely constrained solutions provide us to change and to re-define the geodetic datum for all epoch-wise solutions.

Table 9-5: Results of PAL-GRF GNSS Network Adjustment in Earth-Centered Earth-Fixed Reference Frame (ITRF2020, Epoch 2023.50) (Cartesian Coordinates X-Y-Z)

STA	X	σX	Y	σY	Z	σZ
	(m)	(m)	(m)	(m)	(m)	(m)
PL01	4396745.2369	0.0031	3104035.0189	0.0023	3411392.0666	0.0025
PL02	4389857.6104	0.0030	3129365.0367	0.0023	3396842.9549	0.0025
PL03	4428189.0284	0.0032	3095965.9625	0.0023	3377985.4341	0.0025
PL04	4415160.9898	0.0029	3146759.9405	0.0022	3347577.0491	0.0023
PL05	4436529.0924	0.0031	3115451.9894	0.0023	3349868.0962	0.0025
PL06	4415220.8422	0.0032	3124136.4718	0.0024	3370214.0992	0.0026
PL07	4441009.5692	0.0027	3128091.1964	0.0020	3333092.7445	0.0021
PL08	4450068.6336	0.0030	3143156.3151	0.0023	3306307.9263	0.0024
PL09	4469260.2971	0.0027	3119442.1118	0.0021	3303001.0263	0.0022
PL10	4454113.3760	0.0029	3129394.8574	0.0021	3314533.5676	0.0023

Table 9-6: Results of PAL-GRF GNSS Network Adjustment in Ellipsoidal Coordinate System (ITRF2020, Epoch 2023.55) (Ellipsoidal Coordinates Latitude-Longitude-Ellipsoidal Height)

STA.	Latitude			Std.dev	Longitude			Std.dev	Elip. H	Std.dev
	d	m	s	m	d	m	s	m	m	m
PL01	32	32	33.73654	0.0011	35	13	17.42874	0.0013	140.8009	0.0032
PL02	32	23	17.74073	0.0011	35	29	1.13067	0.0013	-43.0897	0.0031
PL03	32	11	11.21786	0.0011	34	57	33.48289	0.0013	72.0734	0.0032
PL04	31	51	53.14465	0.0010	35	28	41.21388	0.0013	-242.0254	0.0030
PL05	31	53	7.23937	0.0011	35	4	39.28594	0.0013	426.3733	0.0032
PL06	32	6	0.89644	0.0011	35	16	57.31225	0.0014	678.5779	0.0033
PL07	31	42	17.32799	0.0009	35	9	34.27758	0.0012	882.5043	0.0027
PL08	31	25	23.06869	0.0011	35	14	3.07276	0.0013	568.3492	0.0031
PL09	31	23	16.25514	0.0009	34	54	50.99479	0.0012	620.0848	0.0028
PL10	31	30	29.10888	0.0010	35	5	28.73693	0.0013	922.5812	0.0030

10. DETERMINATION VELOCITY FIELD OF THE PAL-GRF STATIONS

10.1. Tectonic Setting of Palestine

The territory of Palestine lies in a tectonically active region. Tectonic structure of the Palestinian territory is mainly formed by the Dead Sea Transform (DST) fault system. The fault system forms the transform boundary between the African Plate to the west and the Arabian Plate to the east. Tectonic structure of the region is given in Figure 10-1.

The DST fault system, also sometimes referred to as the Dead Sea Rift, is a series of faults that run from the Maras Triple Junction (a junction with the East Anatolian Fault in southeastern Turkey) to the northern end of the Red Sea Rift (just offshore of the southern tip of the Sinai Peninsula). It is a zone of left lateral displacement, signifying the relative motions of the two plates, the African Plate and the Arabian Plate. Both plates are moving in a general north-northeast direction, but the Arabian Plate is moving faster, resulting in the observed left lateral motions along the fault at its southern end. A component of extension is also present in the southern part of the transform, which has contributed to a series of depressions, or pull- apart basins, forming the Gulf of Aqaba, Dead Sea, Sea of Galilee, and Hula basins. A component of shortening affects the Lebanon restraining bend, leading to uplift on both sides of the Beqaa valley. There is local trans tension in the northernmost part of the fault system, forming the Ghab pull-apart basin.

In particular, the location of Palestine on the border separating two tectonic plates (Sinai and Arabia) has caused a special and irregular kinematic motion of the earth's crust. There is relatively fast absolute movement in the horizontal directions/components with relatively high velocity, while the vertical component seems to be more stable with slow velocity. The movements and their velocities are not systematically distributed all over the territory due to relative motions of the tectonic plates.

The estimated values for relative motion along the DSF are ranging from 1 to 10 mm/year obtained from different methods (regional plate motion models, local slip rates, seismic forecasts, geomorphological forecasts and space geodesy technologies). The estimated relative plate motion between the two plates based on modern space techniques is about 5 mm/yr. (Figure 10-2).

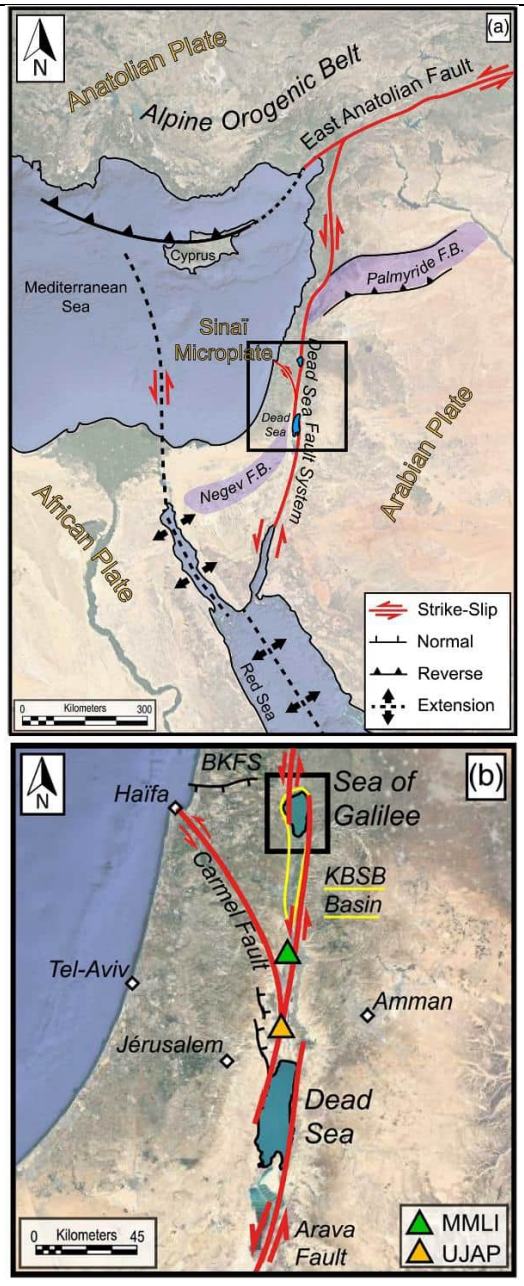

Figure 10-1 : Tectonic structure around the region

Haddad, A. et al. (2019): Tectonics of the Dead Sea Fault Driving the July 2018 Seismic Swarm in the Sea of Galilee(Lake Kinneret), JGR Solid Earth, 10.1029/ 2019JB018963.

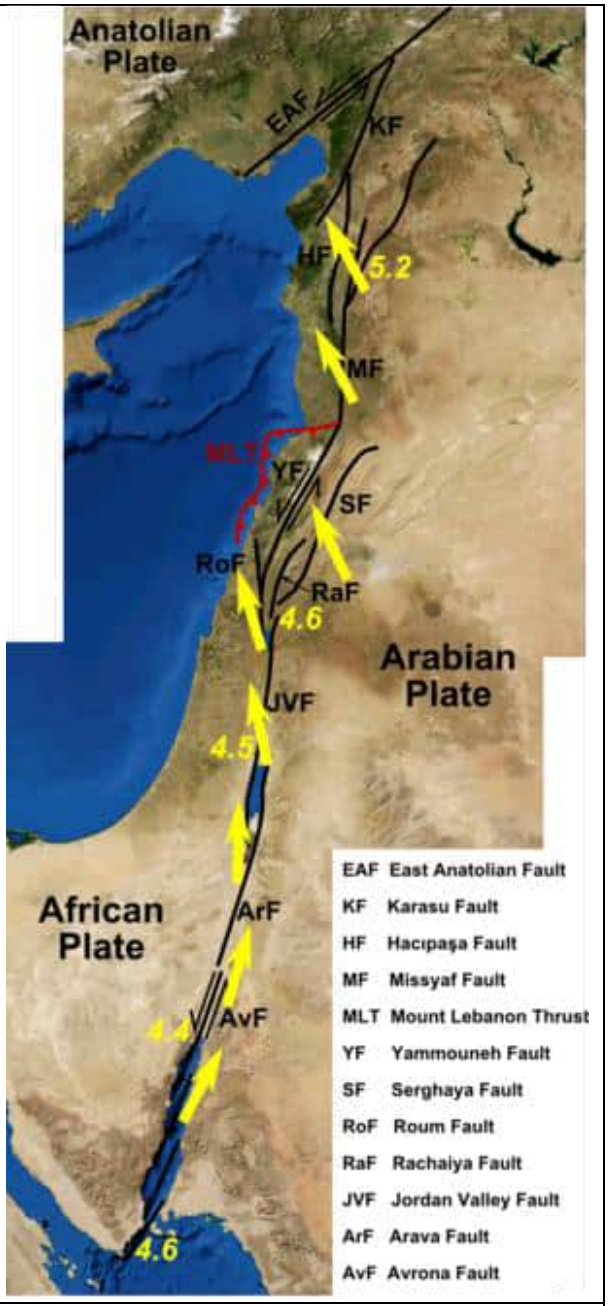

Figure 10-2: : GPS relative velocity field around the region (Arabian versus African, mm/yr)

Gomez, F. et al. (2007): Global Positioning System measurements of strain accumulation and slip transfer through the restraining bend along the Dead Sea fault system in Lebanon. Geophys. J. Int. 168 (3): 1021–1028.

10.2. Estimation of Velocities of PAL-GRF Stations

The coordinate reference frames (geodetic networks) are fixed to the Earth's crust. Thus; the tectonic motion causes the network stations, which are fixed to the ground, move with the time. Moreover, the coordinates of the network stations change in accordance with the crustal motion, and are given with another component, namely the velocity. The modern coordinate reference frames are defined with respect to the center of mass of the Earth and fixed to the crust of the Earth in a time variable space.

The important point in the definition of the PAL-GRF is the management of coordinate changes due to earth crustal movements. This issue plays a critical role in stable and long-term geodetic datum. Historical geodetic networks are usually in the form of static datum in which the coordinates of the stations are held fixed. The existing Palestine Grid 1923 can be an example of this kind of static datum. In this model coordinates do not change while the Earth's crust changes with time. This datum can be adopted if a whole country is under homogeneous deformation, otherwise, the accuracy and stability decrease over time.

In order to determine velocities (annual displacements) at PAL-GRF stations with high accuracy (mm level), at least 2-3 years of continuous GNSS measurements are required at PAL-GRF stations. To achieve similar accuracy with episodic campaign measurements, a much longer time period (more than 6 years) would be required. Currently, the only option is to determine the velocity field of the region and estimate the velocities at PAL-GRF stations based on this velocity field.

There are currently a number of Continuous GNSS stations operating in the immediate vicinity of the country, and some of them have also been included in ITRF2020 solution (Altamimi et all., 2022). This solution includes velocities at some stations around the region. But distribution of these stations is not dense.

In order to investigate the velocity field in the country in more detail, we evaluated approximately 3 years of GNSS data obtained from all suitable Continuous GNSS stations in the close vicinity of the country. Then the velocities at PAL-GRF stations were predicted based on the computed velocity field.

For this purpose, we formed network of 50 CORS stations located in the vicinity of the country, 8 of them (ALON, BSHM, CSAR, DRAG, ELAT, KABR, RAMO and TELA) included in the ITRF2020 solution. 3-year daily data of these stations covering the period 2019-2021 were downloaded from the internet, as well as IGS precise orbit, earth rotation parameters, ionospheric files, etc. was arranged and made ready for the GNSS processing. Stations containing data for less than a year were excluded from evaluation.

First, preliminary quality control of the data was carried out and measurements with a duration of less than 8 hours and measurements with a multipath error greater than 1 m were excluded from evaluation. Then, daily data were processed with Bernese V5.2 software by following the method explained in detail in Chapter 8, and loosely constrained (free) daily solutions were obtained.

To check the consistency and quality of the daily solutions, a minimally constrained solution (No-Net-Translation) using fiducial stations is applied. Quality of the solutions is checked with the long-term coordinate repeatability (time series analysis) of the stations. The coordinates from the daily solutions are compared with the estimated model and difference from the model value is calculated for each component (north, east and up) separately.

Time series of 8 datum defining ITRF2020 stations were examined to define a suitable datum for daily free solutions and to calculate daily coordinates of the stations. From the 8 stations, BSHM and ELAT were excluded due to their inappropriate behaviors and remaining 6 stations (ALON, CSAR, DRAG, KABR, RAMO and TELA) were used for datum definition and the station coordinates were calculated for each daily solution. There is no event detected in the time series of the remaining fiducial stations.

Time series of coordinates resulting from the processing of individual daily sessions can be analyzed and modelled in local components (North, East, and Up) or in global components (X, Y, Z). The coordinate components both in local and global for each station were analyzed separately and the

effects on station coordinates and time-dependent coordinate changes were modeled. The functional model including station coordinate at reference epoch, discontinuities, one or more linear velocities, and a set of periodic functions is adapted to the time series of the data according to the significance of the components. Parameters that were found to be statistically insignificant were eliminated from the model. Outliers are also identified and removed from the data using statistical test.

The mathematical model for each component $X(t_i)$ can be written as follows:

$$X(t_i) = X_0 + V_0(t_i - t_0) + \sum_{k=1}^{n_o} O_k \, H_{o,k}(t_i) + \sum_{k=1}^{n_v} V_k \, (t_i - t_k) \, H_{v,k}(t_i) + \sum_{k=1}^{n_p} (A_k \cos(w_k \, (t_i - t_0)) + B_k \cos(w_k \, (t_i - t_0))) \, H_{p,k}(t_i)$$

Where;

X_0 , station coordinate at an epoch t_0
V_0 , V_k , one or more station velocities
O_k , discontinuities
$H_{p,k}$, periodic functions with the predefined frequency w_k and the parameters (A_k and B_k)

As a result, the behavior of the stations was revealed by time series analysis of a total of 1095 daily solutions for 50 stations and the coordinates were calculated in the ITRF2020 reference frame. As an example, results of time series analysis for IGS stations, RAMO and ELAT are given in **Hata! Başvuru kaynağı bulunamadı.** Figure 10-4. As seen in Figure 10-4, ELAT station has been removed from the datum defining stations due to displacement occurred on April 2019 and January 2020. The results for the other stations are given in Appendix-I.

At some points, there are jumps in the time series, which most probably arisen from the antenna changes. However, the magnitude of these changes is generally less than 1 cm, and in only a few points it is more than 1 cm and less than 2 cm. Another interesting result is that the behavior of some stations is quite abnormal, which cannot be used as a reference for high accurate positioning.

Horizontal velocities obtained as a result of time series analysis of daily solutions are shown in the Figure 10-5. Stations containing data for a period of two years or less are not included in this figure.

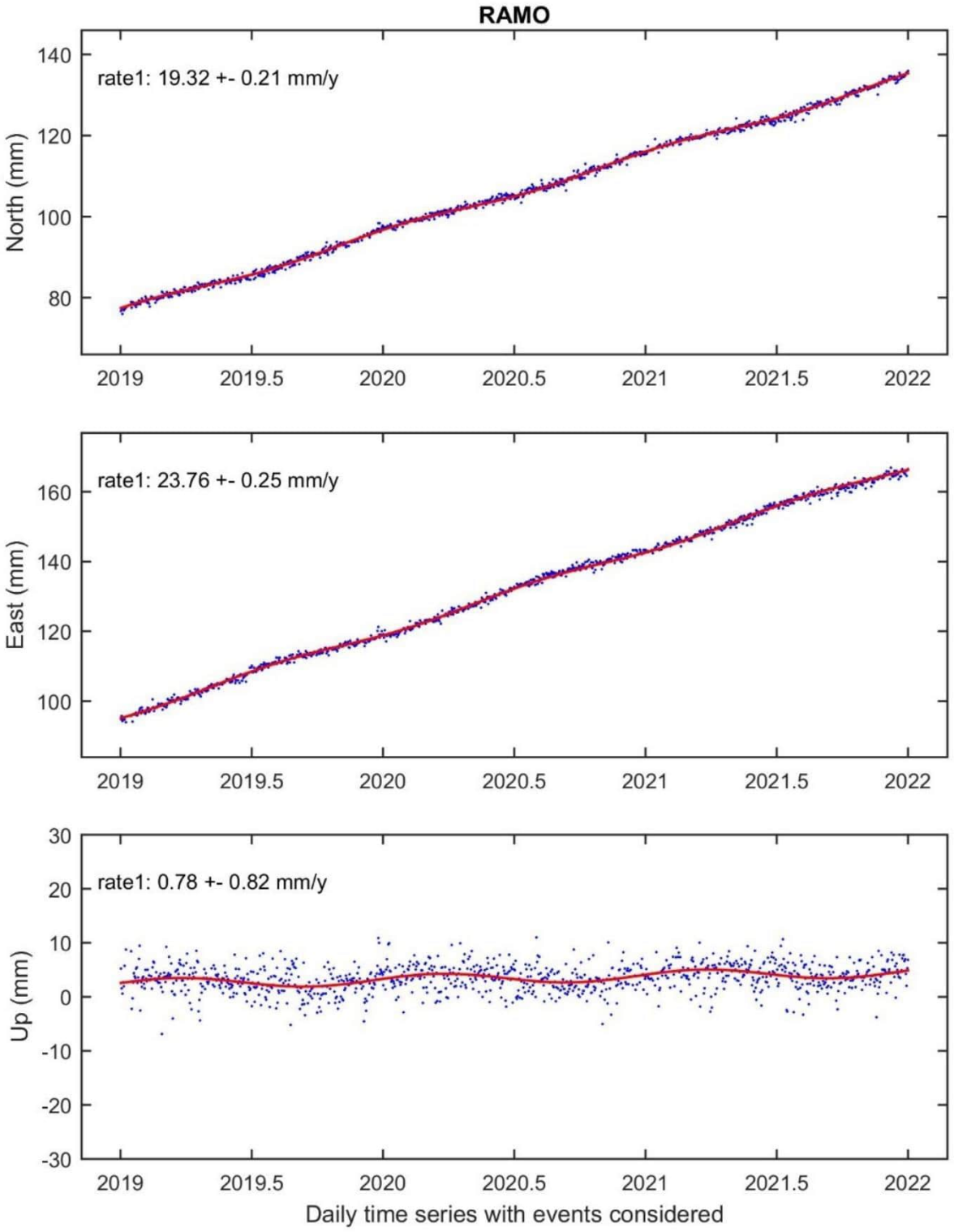

Figure 10-3 : Velocity components of RAMO IGS station computed in ITRF2020.

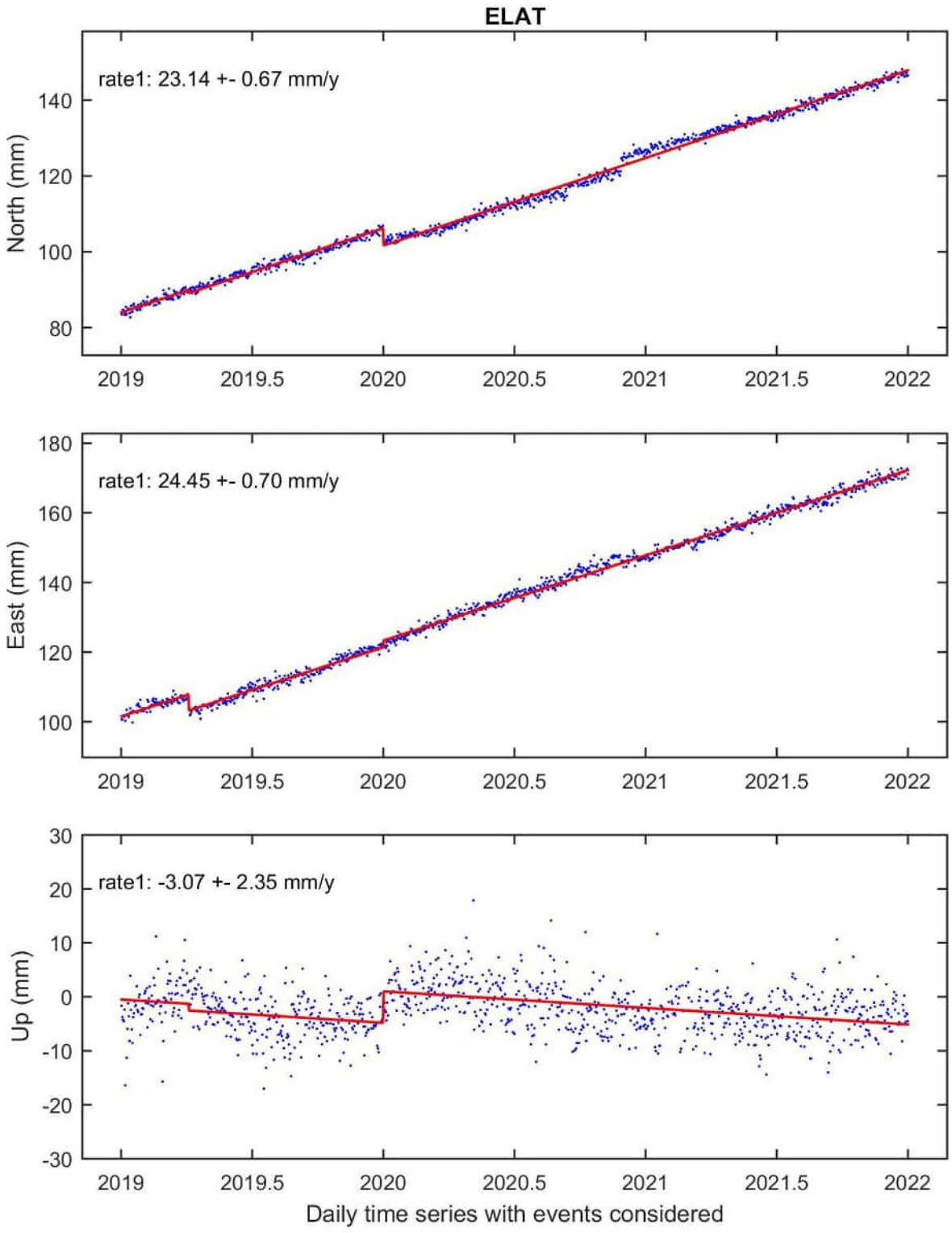

Figure 10-4 : Velocity components of ELAT IGS station computed in ITRF2020.

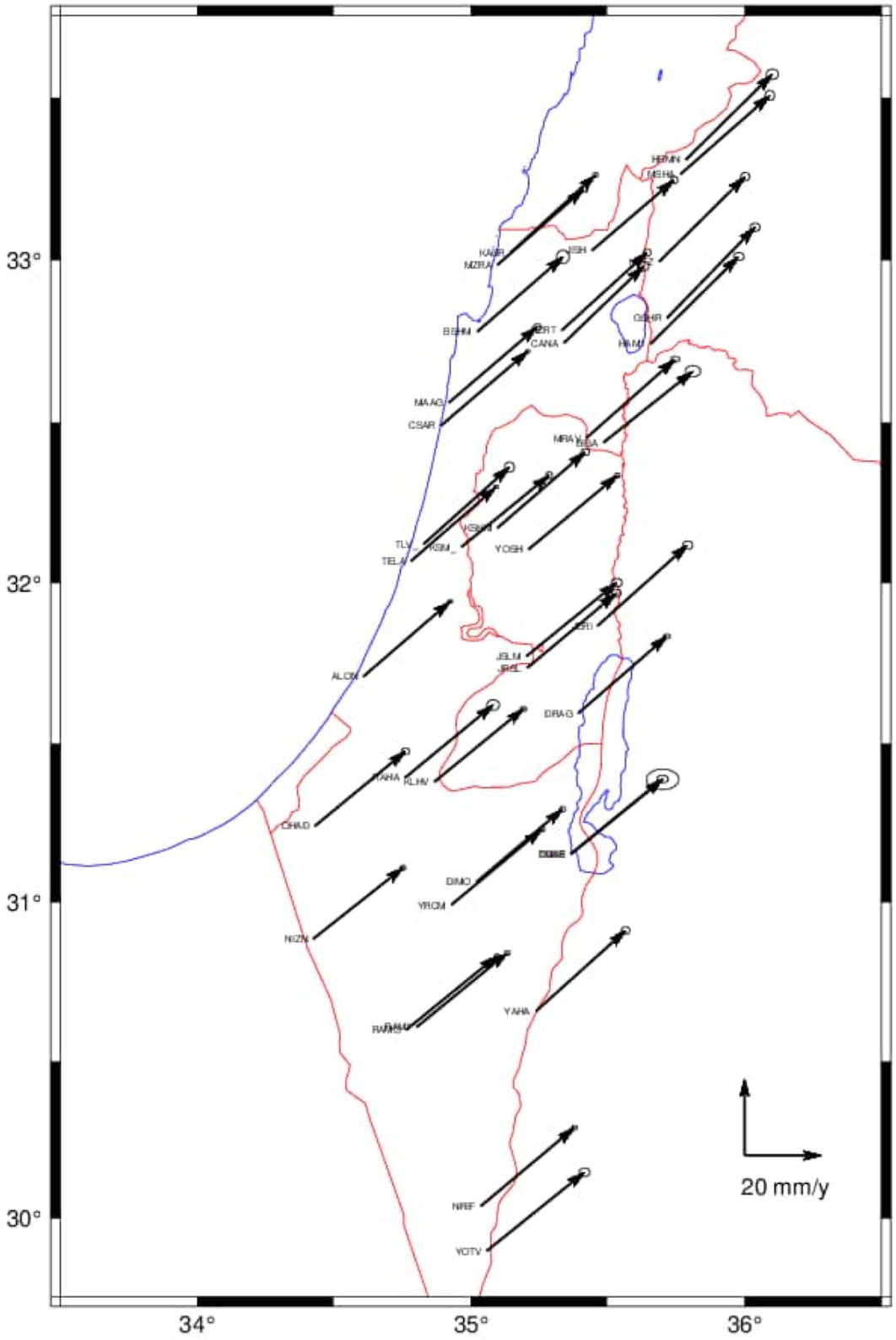

Figure 10-5: Horizontal velocity field calculated by time series analyses

By using the velocity components (VX, VY and VZ) calculated based on time series analyses, the velocity values at the PAL-GRF points were predicted by the Kriging method. Table 10-1 gives the predicted velocity components at PLA-GRF stations.

Table 10-1: Predicted velocity components at PAL-GRF stations

Station	Longitude (deg)	Latitude (deg)	h (m)	VX (m)	VY (m)	VZ (m)	Velocity vector
PL01	35.22150	32.54270	140.8	-0.022	0.012	0.017	0.030
PL02	35.48364	32.38826	-43.08	-0.021	0.014	0.017	0.030
PL03	34.95930	32.18644	72.07	-0.022	0.012	0.016	0.030
PL04	35.47811	31.86476	-242.02	-0.022	0.013	0.018	0.032
PL05	35.07757	31.88534	426.37	-0.021	0.013	0.017	0.030
PL06	35.28258	32.10024	678.57	-0.021	0.014	0.017	0.031
PL07	35.15952	31.70481	882.5	-0.020	0.014	0.018	0.030
PL08	35.23418	31.42307	568.34	-0.020	0.014	0.018	0.030
PL09	34.91416	31.38784	620.08	-0.020	0.014	0.017	0.030
PL10	35.09131	31.50808	922.58	-0.020	0.014	0.018	0.030

In the last column of Table 10-1, the magnitudes of the estimated velocities at the PAL-GRF stations are given. It can be seen that the velocity difference of the PAL-GRF stations relative to each other is less than 1 mm/year and only at one station it reaches a maximum of 2 mm/year. This result can be expressed as an indicator that the entire country moves at the same constant amount with respect to the center of the earth.

It can be concluded that the velocity differences at these points are negligible and no practical meaning. Therefore, it would be more appropriate to use the ITRF2020 coordinates of PAL-GRF stations (epoch: 2023.5) directly without taking into account the velocity values.

Hence, the static datum is suitable for Palestine because of that the relative motion of network stations causes negligible degradation of positioning accuracy and datum stability. For that reason, the implementation of a static datum for Palestine is proposed. The new datum will be referred to a specific epoch (2023.5) and include a zero-velocity model.

In other words, the PAL-GRF coincides with the ITRF2020 (Altamimi et all. 2022) at campaign measurement epoch 2023.5 and co-moving with the crust. It means that PAL-GRF coordinates are defined in the ITRF2020 at epoch 2023.5 but diverge with respect to ITRF2020 at any epoch different from 2023.5 due to the crustal motions.

11. DATUM TRANSFORMATIONS AND COORDINATE TRANSFORMATION & CONVERSIONS

Palestine geodetic datum was originally established using classical surveying techniques, and it will be integrated with the global geodetic reference systems within this project. A brief summary of the coordinate reference frames/datums/projections currently in use in the territory is given below. Since a new reference frame (PAL-GRF) has been established, all necessary conversions, transformations and computations have been facilitated for the geospatial data (surveying, mapping, cadaster, GIS etc.) community

Table 11-1: Coordinate reference frames/datums/projections used in Palestine

Coordinate type	OLD (existing)	NEW (established)
3-D Cartesian coordinates	N/A	PAL-GRF (ITRF2020)
2-D ellipsoidal coordinates	N/A	PAL-GRF ITRF2020 GRS80 ellipsoid
2-D grid (projection) coordinates	Palestine 1923 Grid (EPSG: 28191) Cassini-Soldner	PAL-GRF Transverse Mercator

PAL-GRF has been defined aligned to ITRF2020 and provides 3-dimensional coordinates to the user community. Coordinates in PAL-GRF may be described in various types of coordinates given below;

- 3-D Cartesian coordinates
- 2-D ellipsoidal coordinates
- 2-D grid (projection) coordinates
- 1-D orthometric heights (with given geoid model)

Given the 3-D cartesian coordinates all other coordinate components can be computed by using well known conversion equations. Orthometric heights can only be computed with a geoid model compatible with the PAL-GRF.

The conversion between the PAL-GRF coordinate components and the ‘existing (old) coordinates may be carried out by means of datum transformation models. Datum transformation may be applied in 3-D or 2-D. according to the definition of coordinates to be transformed into each other. In the case of Palestine geodetic networks, the transformations given below will be implemented for practical use. Although the datum transformation models are well known and applied in the literature, mathematical equations and algorithms of transformation models are given in this document.

11.1. GNSS measurements on the PLA1923 trig points

In order to determine the datum transformation parameters between PAL-GRF and PAL1923, GNSS measurements were made at 53 old triangulation points with known Cassini-Soldner projection coordinates in PAL1923 datum. During these measurements, some selected PAL-GRF points were also

occupied simultaneously. The distribution of the common points throughout the country on which GNSS measurements were carried out is shown in Figure 11-1. It can be said that these common points show a good distribution across the country.

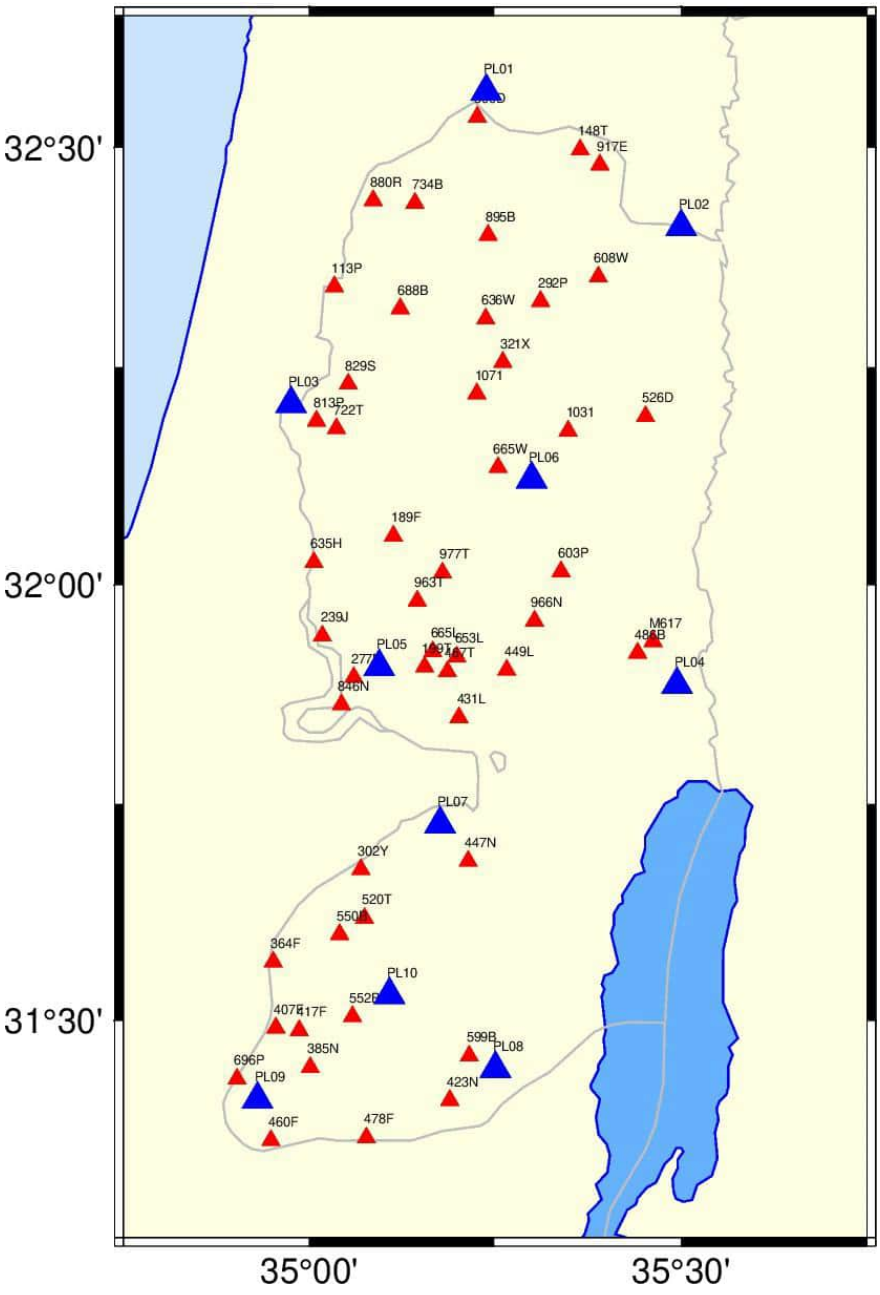

Figure 11-1 : Distribution of PAL1923 points measured by GNSS (Blue triangle PLA-GRF station, red triangle old trig points)

GNSS measurements at PAL1923 trig points were carried out in 3 groups and a total of 14 sessions during 8 August - 6 September 2023. In order to ensure high accuracy, each point was visited twice and at least 4 hours of GNSS data were collected. Observation plan is given in Table 11-2. It shows that at least two PAL-GRF stations were permanently observed in order to provide fiducial stations for geodetic datum definition.

A total of 11 geodetic GNSS receivers with double frequency (10 Trimble R8S and 1 Trimble R8-4) were used for all observations. The observation parameters are given in Table 11-3

The collected data have been quality checked by using TEQC software, similar to the method described above in the PLA-GRF data quality check. GNSS data and summary of the quality check of all data files are given in Appendix-J. The results of the “teqc” process clearly show that all GNSS data collected at the old trigonometric points are of good quality for the post-processing.

Table 11-2: GNSS observation plan

Year	Mo	Day	Doy & Session#	Stations Measured											Group
2023	8	9	2210	447N	449L	608W	696P	813P	846N	M617	PL01	PL08			Group 1
2023	8	13	2250	1071	199T	302Y	417F	467T	486B	552B	722T	PL01	PL08		
2023	8	15	2270	113P	170L	321X	478F	520T	635H	636W	653L	PL01	PL08		
2023	8	16	2280	022Y	1031	423N	431L	526D	813S	977T	PL01	PL08			
2023	8	21	2330	447N	449L	608W	696P	813P	846N	M617	PL01	PL08			
2023	8	23	2350	1071	199T	302Y	417F	467T	486B	552B	722T	PL01	PL07		Group 2
2023	8	28	2400	113P	170L	321X	478F	520T	635H	636W	653L	PL01	PL07		
2023	8	29	2410	022Y	1031	423N	431L	599B	813S	977T	PL01	PL07			
2023	9	4	2470	189F	277B	364F	460F	599B	665L	829S	895B	966N	PL01	PL10	Group 3
2023	9	4	2471	189F	277B	364F	460F	599B	665L	829S	895B	966N			
2023	9	5	2480	148T	239J	385N	407F	550B	603P	665W	880R	963T	PL01	PL10	
2023	9	5	2481	148T	239J	385N	407F	550B	603P	665W	880R	963T			
2023	9	6	2490	292P	688B	734B	800D	917E	PL01	PL10					
2023	9	6	2491	292P	688B	734B	800D	917E							

Table 11-3: GNSS observation parameters

Parameter	Criteria
Duration	PAL_GRF stations continuously Other stations 4 hours at least
Measurement number	2 times/station
Sampling rate	10 seconds
Minimum number of satellites to be observed	5
Antenna height measurement	At the beginning and end of the session
Precision of the antenna height measurement	mm

Data for each session were processed separately following the same methodology described above (Chapter 8), resulting in loosely constrained (free) normal equations containing only the coordinates. Then, the campaign solution was obtained by combining the session solutions and ITRF2020 coordinates were computed based on PAL-GRF stations. The ITRF2020 and PAL1923 coordinates of trig points are given in Table 11.4 and Table 11.5 respectively. Moreover, Appendix-J includes all station coordinates used in the datum transformation. The quality of the combined solution was checked by coordinate repeatability given in Table 11-6.

Table 11-6 shows that coordinate repeatability, except for a few points, is generally at the level of 1 cm for horizontal components and a few cm for vertical components. The average repeatability values are 5 mm, 6 mm and 15 mm for the north, east and up components, respectively. This indicates that the obtained coordinates are of high accuracy.

Table 11-4: The ITRF2020 coordinates of trig points used in the datum transformation

Station Name	Longitude	Latitude	Elipsoidal Height	X	Y	Z	Transversal Mercator	
	deg	deg	m	m	m	m	Easting (m)	Northing(m)
022Y	35.26221304	32.03197218	868.118	4419744.989	3124979.803	3363897.940	222570.56	528186.79
1031X	35.34820952	32.17660381	597.728	4407909.768	3126545.620	3377341.308	230677.00	544230.14
1071X	35.22567569	32.21942691	786.2689	4412649.300	3115744.026	3381460.585	219121.02	548973.24
113P	35.03409585	32.34169000	147.8046	4416671.429	3096505.184	3392582.933	201086.60	562548.95
148T	35.36437648	32.49756667	300.4518	4391295.916	3116624.202	3407257.002	232158.75	579824.45
170L	35.53958386	32.19211837	-196.9022	4396149.256	3140327.480	3378374.148	248721.06	545985.61
189F	35.11333211	32.05674030	498.4021	4426401.695	3112466.194	3366030.045	208510.27	530939.43
199T	35.15543330	31.90661626	783.8077	4431520.741	3120934.540	3352059.743	212473.86	514288.94
239J	35.01771626	31.94200758	281.5503	4436960.654	3108838.328	3355125.239	199455.18	518231.18
277B	35.05995374	31.89454959	371.9664	4437008.040	3113750.736	3350706.075	203440.37	512961.52
292P	35.31140882	32.32471095	558.9696	4402737.897	3118628.556	3391211.833	227194.57	560650.92
302Y	35.06977020	31.67385859	638.2387	4447209.900	3122047.389	3330043.501	204331.85	488489.06
321X	35.26060925	32.25540332	649.6796	4408916.599	3117138.488	3384762.570	222413.17	552962.96
364F	34.95186309	31.56783019	485.8365	4458571.420	3116346.182	3319951.669	193120.64	476755.48
385N	35.00147213	31.44614668	733.9908	4461821.068	3124371.596	3308577.249	197801.51	463252.22
407F	34.95527316	31.49192745	506.8976	4462008.058	3119143.562	3312788.606	193422.89	468338.59
417F	34.98659336	31.48896885	766.4019	4460624.041	3121807.356	3312644.400	196397.92	468003.38
423N	35.18926429	31.40845520	742.8119	4453343.906	3140239.043	3305015.387	215650.76	459050.40
431L	35.20169332	31.84845827	813.6891	4431803.432	3126489.577	3346598.626	216847.57	507837.81
447N	35.21392250	31.68356038	716.6254	4438933.871	3132939.048	3331000.230	218001.51	489553.14
449L	35.26582687	31.90308822	775.2955	4425662.251	3129582.309	3351723.097	222916.00	513895.38
460F	34.94852577	31.36196637	484.9593	4468518.941	3122911.644	3300480.354	192744.24	453930.44
467T	35.18587274	31.90107708	826.4816	4430157.002	3123496.375	3351560.802	215352.82	513673.02
478F	35.07688709	31.36504271	780.8424	4461572.852	3132957.906	3300925.632	204957.32	454246.88
486B	35.44190359	31.92243198	-78.3031	4414509.650	3142090.384	3353092.700	239567.49	516058.59
520T	35.07456984	31.61793527	868.71	4449771.813	3124402.409	3324885.001	204777.87	482287.54
526D	35.45250481	32.19305702	-95.128	4400941.885	3133660.310	3378516.453	240509.61	546069.76
550B	35.04115785	31.59929961	661.2657	4452335.195	3122327.448	3323016.285	201603.97	480226.34
552B	35.05837849	31.50486193	933.4488	4456072.138	3126946.469	3314234.442	203221.35	469752.36
599B	35.21539578	31.45942898	631.076	4449425.006	3140514.953	3309780.005	218136.74	464701.50
603P	35.33895661	32.01572007	747.3926	4416251.494	3131390.544	3362305.814	229821.54	526389.04
608W	35.38900389	32.35263916	374.2899	4397032.443	3123538.420	3393729.924	234496.39	563755.82
635H	35.00661007	32.02625192	261.0536	4433495.872	3105129.547	3363038.185	198424.78	527574.97
636W	35.23741201	32.30467424	622.6723	4407776.089	3113656.301	3389367.914	220227.16	558426.43
653L	35.19869663	31.91792809	816.5355	4428643.710	3123913.607	3353141.913	216566.52	515541.07
665L	35.16633887	31.92405696	677.9231	4430017.266	3121137.287	3353645.522	213506.63	516222.16
665W	35.25416510	32.13495860	629.0611	4415064.599	3120740.447	3373447.974	221808.32	539606.65
688B	35.12259953	32.31638591	292.4094	4413210.421	3104257.508	3390289.108	209415.53	559730.71
696P	34.90295792	31.43296027	487.1929	4467639.314	3117011.256	3307200.974	188432.57	461814.25
722T	35.03672694	32.17945468	272.8046	4424478.655	3102281.845	3377435.862	201301.07	544557.89
734B	35.14246117	32.43683496	299.7061	4406290.114	3101673.496	3401574.153	211297.40	573085.98
800D	35.22620152	32.53495888	133.7291	4396863.497	3104658.240	3410664.112	219173.47	583963.76
813P	35.01012846	32.18821046	152.2555	4425411.201	3099872.284	3378193.420	198794.61	545533.75
813S	35.06509241	32.26075852	288.9226	4419018.720	3101717.952	3385072.246	203990.44	553569.19
829S	35.05275498	32.23034346	258.3844	4421138.566	3101785.074	3382203.253	202822.22	550198.32
846N	35.04355907	31.86328426	266.1845	4439324.375	3113480.792	3347706.132	201883.29	509497.28
880R	35.08618063	32.43983590	174.8879	4409102.427	3097180.625	3401788.075	206005.09	573424.75
895B	35.24076532	32.40013629	373.3833	4402794.791	3110523.787	3398178.039	220542.41	569012.54
917E	35.39099056	32.48037309	346.2601	4390714.211	3119279.187	3405673.243	234662.72	577921.10
963T	35.14555432	31.98219741	637.3511	4428330.877	3117545.957	3359094.742	211546.34	522670.58
966N	35.30330205	31.95921462	842.3599	4420974.118	3130606.693	3357041.119	226456.95	520120.63
977T	35.17922512	32.01431845	700.327	4424998.874	3119091.071	3362149.065	214730.46	526230.25
M617	35.46248122	31.93569639	-121.03	4412717.789	3143203.309	3354318.384	241510.49	517533.34

Table 11-5: The PAL1923 coordinates of trig points used in the datum transformation

Station Name	Longitude	Latitude	Elipsoidal Height	X	Y	Z	PAL1923 Grid (Cassini -Soldner)	
	deg	deg	m	m	m	m	Easting (m)	Northing(m)
022Y	35.26142030	32.03166780	868.118	4419984.275	3125057.264	3363637.969	174912.41	159863.78
1031X	35.34741096	32.17632199	597.728	4408148.421	3126622.550	3377082.986	183015.34	175910.64
1071X	35.22487694	32.21914138	786.2689	4412888.382	3115820.649	3381201.776	171457.89	180650.76
113P	35.03329121	32.34139955	147.8046	4416911.528	3096580.998	3392323.272	153419.40	194221.65
148T	35.36354881	32.49730720	300.4518	4391535.588	3116698.912	3406999.744	184487.06	211506.32
170L	35.53879155	32.19187790	-196.9022	4396385.340	3140404.307	3378119.659	201060.26	177674.34
189F	35.11255782	32.05644304	498.4021	4426639.877	3112544.276	3365770.664	160852.72	162614.21
199T	35.15465447	31.90630092	783.8077	4431759.715	3121012.720	3351799.152	164819.45	145963.22
239J	35.01695221	31.94169399	281.5503	4437198.989	3108917.103	3354864.699	151800.86	149902.83
277B	35.05918114	31.89422671	371.9664	4437247.142	3113829.230	3350444.816	155786.46	144633.18
292P	35.31059662	32.32443661	558.9696	4402977.232	3118704.357	3390953.734	179528.10	192330.87
302Y	35.06902490	31.67353099	638.2387	4447447.324	3122127.703	3329782.528	156685.55	120161.41
321X	35.25981389	32.25511330	649.6796	4409155.726	3117215.753	3384503.224	174749.68	184640.50
364F	34.95113328	31.56749482	485.8365	4458808.335	3116427.235	3319690.320	145477.80	108425.20
385N	35.00074697	31.44580449	733.9908	4462057.754	3124453.170	3308315.665	150162.00	94922.72
407F	34.95454860	31.49158564	506.8976	4462244.844	3119225.083	3312526.904	145782.26	100008.02
417F	34.98586864	31.48862852	766.4019	4460860.718	3121888.936	3312382.847	148757.44	99673.59
423N	35.18853166	31.40811756	742.8119	4453580.445	3140320.576	3304754.363	168012.08	90725.19
431L	35.20092844	31.84815038	813.6891	4432041.121	3126568.646	3346338.929	169195.98	139514.08
447N	35.21317004	31.68324133	716.6254	4439171.096	3133019.138	3330740.031	170354.86	121229.17
449L	35.26504605	31.90277980	775.2955	4425900.845	3129660.555	3351463.170	175261.91	145572.58
460F	34.94780957	31.36161869	484.9593	4468755.309	3122993.692	3300218.540	145107.30	85599.72
467T	35.18509322	31.90076355	826.4816	4430395.876	3123574.556	3351300.400	167698.59	145348.11
478F	35.07616538	31.36470160	780.8424	4461809.035	3133039.842	3300664.427	157320.22	85919.33
486B	35.44112380	31.92214443	-78.3031	4414746.977	3142168.781	3352834.677	191913.71	147741.42
520T	35.07383107	31.61760493	868.71	4450008.901	3124483.215	3324623.956	157133.47	113959.94
526D	35.45170141	32.19278291	-95.128	4401180.313	3133737.079	3378258.804	192847.49	177753.07
550B	35.04041884	31.59896818	661.2657	4452572.358	3122408.093	3322755.202	153959.84	111898.07
552B	35.05764748	31.50452599	933.4488	4456308.879	3127027.744	3313973.249	155580.17	101424.37
599B	35.21466311	31.45910445	631.076	4449660.986	3140596.268	3309520.047	170497.02	96378.00
603P	35.33817388	32.01542839	747.3926	4416489.491	3131468.630	3362047.091	182165.00	158068.99
608W	35.38818958	32.35237131	374.2899	4397271.522	3123614.223	3393472.345	186829.37	195437.88
635H	35.00583515	32.02594274	261.0536	4433734.751	3105207.473	3362777.785	150767.48	159246.50
636W	35.23661314	32.30438542	622.6723	4408015.466	3113733.268	3389108.523	172562.12	190103.43
653L	35.19792561	31.91762650	816.5355	4428881.562	3123992.132	3352882.580	168912.76	147217.66
665L	35.16555770	31.92374361	677.9231	4430256.288	3121215.305	3353385.062	165851.65	147896.79
665W	35.25337539	32.13466689	629.0611	4415303.300	3120817.910	3373188.859	174148.08	171284.42
688B	35.12179640	32.31609870	292.4094	4413450.121	3104333.641	3390029.831	161749.37	191405.61
696P	34.90224130	31.43261360	487.1929	4467875.859	3117093.208	3306939.014	140793.86	93482.42
722T	35.03593821	32.17915461	272.8046	4424718.074	3102358.862	3377175.820	153639.08	176230.31
734B	35.14164220	32.43655809	299.7061	4406530.348	3101748.408	3401315.460	163627.07	204761.87
800D	35.22536994	32.53468942	133.7291	4397104.107	3104732.499	3410405.801	171500.02	215641.67
813P	35.00933862	32.18790713	152.2555	4425650.888	3099949.235	3377933.043	151132.23	177205.26
813S	35.06423828	32.26046204	288.9226	4419261.611	3101790.102	3384812.278	156320.54	185242.20
829S	35.05196050	32.23004697	258.3844	4421378.191	3101861.706	3381943.382	155158.59	181871.22
846N	35.04280116	31.86296686	266.1845	4439562.381	3113560.103	3347445.493	154231.42	141169.37
880R	35.08535695	32.43954567	174.8879	4409343.644	3097255.402	3401528.123	158334.03	205098.05
895B	35.23994998	32.39986419	373.3833	4403034.407	3110599.143	3397919.910	172873.64	200691.04
917E	35.39016828	32.48011512	346.2601	4390953.454	3119354.331	3405416.180	186992.03	209603.73
963T	35.14476864	31.98188669	637.3511	4428570.151	3117623.582	3358834.339	163889.53	154344.83
966N	35.30252455	31.95891847	842.3599	4421211.993	3130685.059	3356782.161	178802.05	151799.66
977T	35.17844649	32.01402064	700.327	4425237.156	3119169.015	3361889.770	167073.72	157906.44
M617	35.46170321	31.93541289	-121.03	4412954.819	3143281.821	3354060.698	193856.65	149216.95

Table 11-6 : Coordinate repeatability of the old trig points

Station	# of obs	N	E	U		Station	# of obs	N	E	U
022Y	2	6.6	5.8	9.6		599B	3	9.2	3.5	20.4
1031	2	6.9	2.5	15.5		603P	2	1.5	7.8	14.7
1071	2	9.1	2.4	6.8		608W	2	4.4	2.5	1.3
113P	2	3.1	3.7	21.7		635H	2	5.2	6.3	5.6
148T	2	9.5	4.7	15.4		636W	2	6.0	3.7	28.4
170L	2	4.9	2.2	6.9		653L	2	11.1	6.9	11.6
189F	2	2.4	4.4	7.6		665L	2	1.8	4.7	9.6
199T	2	7.9	7.9	7.1		665W	2	5.7	6.3	2.9
239J	2	2.9	8.0	2.9		688B	2	10.2	4.1	7.7
277B	2	6.2	4.7	27.7		696P	2	6.3	2.8	13.4
292P	2	7.2	7.9	6.8		722T	2	7.5	2.8	4.8
302Y	2	12.9	6.1	9.8		734B	2	6.6	5.3	6.4
321X	2	5.0	7.6	18.2		800D	2	7.1	6.2	19.5
364F	2	2.3	5.0	10.8		813P	2	4.1	3.8	9.4
385N	2	5.1	8.2	3.0		813S	2	5.1	3.5	7.4
407F	2	10.8	8.2	32.8		829S	2	8.5	5.1	20.2
417F	2	5.0	4.4	13.9		846N	2	4.0	4.1	11.0
423N	2	3.8	3.6	8.9		880R	2	3.5	7.1	14.8
431L	2	15.8	5.6	8.7		895B	2	6.7	3.1	6.9
447N	2	3.6	3.1	8.2		917E	2	8.0	7.5	11.7
449L	2	14.4	6.4	7.8		963T	2	4.0	5.2	7.9
460F	2	7.1	5.3	12.9		966N	2	2.5	15.1	10.8
467T	2	7.7	9.7	12.9		977T	2	7.0	5.4	11.2
478F	2	9.2	2.7	14.1		M617	2	3.8	8.4	3.2
486B	2	1.4	5.1	7.1		PL01	14	4.6	2.5	8.7
520T	2	0.5	2.4	47.2		PL07	3	2.7	2.2	15.8
526D	1	0.4	0.8	3.8		PL08	5	3.2	2.5	4.0
550B	2	1.1	6.2	27.2		PL10	6	6.7	2.5	10.9
552B	2	5.6	5.0	78.6						
Total							**134**	**6.4**	**5.0**	**16.2**

11.2. Datum Transformation between PAL-GRF and PAL1923

The PAL-GRF was defined by GNSS measurements in the ITRF2020 three-dimensional, geocentric coordinate system based on the GRS-80 ellipsoid. Whereas, the old network PLA1923 was defined by terrestrial measurements (angle, base, astronomical latitude, astronomical longitude, astronomical azimuth) based on Clark1880 ellipsoid and in a different horizontal coordinate system. Additionally, information on old trig point heights is not available.

As a result, since ellipsoid and coordinate systems (datum) are different from each other, it is expected that there will be differences in offset, rotation and scale between these two coordinate systems.

For 3D datum transformation between both systems, ellipsoid heights in the PAL1923 system are needed. Since there was no information about the height, the ellipsoid heights obtained in the PAL-GRF system had to be taken for PAL1923 as well.

The 4-parameter Helmert method was applied for two-dimensional transformation. Additionally, an alternative method based on calculating transformation values from the grid data obtained by the projection coordinate differences between both systems was also applied. Below, some brief theoretical explanations about these methods applied and the results obtained are given.

11.2.1. Three-dimensional similarity transformation (7-parameters, Bursa-Wolf)

Three-dimensional Helmert transformation is defined by seven parameters and is therefore also called 7-parameter transformation. This transformation reflects the relationship between Cartesian three-dimensional coordinate systems, usually geocentrically located. These seven parameters are defined below and shown in Figure 11-2.

- 3 translations along each axis: ΔX, ΔY, ΔZ
- 3 rotations; around each coordinate axis (counterclockwise): R_X, R_Y, R_Z
- A scale factor in ppm: δ

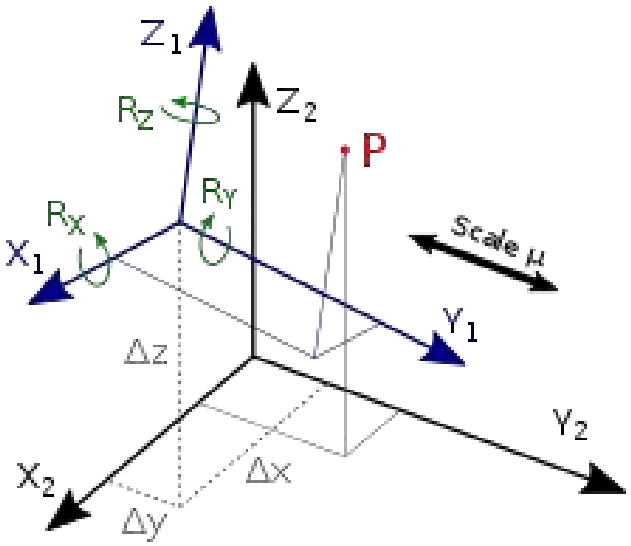

Figure 11-2: Three-Dimensional Datum Transformation

The equations are given below in matrix form.

$$\begin{bmatrix} X \\ Y \\ Z \end{bmatrix}_2 = \begin{bmatrix} \Delta X \\ \Delta Y \\ \Delta Z \end{bmatrix} (1+\delta) \quad \mathrm{R} \begin{bmatrix} X \\ Y \\ Z \end{bmatrix}_1$$

Where R is the rotation matrix according to:

$$R = R_Z R_Y R_X = \begin{bmatrix} cosR_Z & sinR_Z & 0 \\ -sinR_Z & cosR_Z & 0 \\ 0 & 0 & 1 \end{bmatrix} \begin{bmatrix} cosR_Y & 0 & -sinR_Z \\ 0 & 1 & 0 \\ sinR_Z & 0 & cosR_Y \end{bmatrix} \begin{bmatrix} 1 & 0 & 0 \\ 0 & cosR_X & sinR_Z \\ 0 & -sinR_Z & cosR_X \end{bmatrix}$$

The inverse of the transformation is set up as below:

$$\begin{bmatrix} X \\ Y \\ Z \end{bmatrix}_1 = \frac{R^{-1}}{(1+\delta)} \left[\begin{bmatrix} X \\ Y \\ Z \end{bmatrix}_2 - \begin{bmatrix} \Delta X \\ \Delta Y \\ \Delta Z \end{bmatrix} \right]$$

Where R^{-1} is the inverse matrix of R. One important point should be emphasized here. Due to the very large rotation angles and scale between the two systems (angles 5-10 arc-seconds and scale > 10 ppm), the transformation matrices were taken into account in the calculations in their original form without any approximation.

In the 3D transformation, PAL-GRF point coordinates were assumed to be error free since they had very high accuracy compared to PAL1923. Transformation parameters were calculated by the least square method, using PAL1923 coordinates as measurements in the indirect model.

As a result of the preliminary adjustment with 53 common points, 3 points (022Y, 170L and 813S) were detected as outliers and removed. The parameters calculated with the remaining 50 points are given below. The 3D coordinates used in both systems and the post-fit residuals are given in Appendix-J. The post-fit residuals are also shown in Figure 11-3.

3D Transformation Parameters (PAL-GRF to PAL1923)

$\Delta X = \quad 114.5200 \pm 14.8542$ m

$\Delta Y = \quad 79.3790 \pm 9.1074$ m

$\Delta Z = -281.6324 \pm 0.5174$ m

$R_X = -10.07015 \pm 0.51744$ arcsec

$R_Y = \quad -8.45655 \pm 0.28998$ arcsec

$R_Z = \quad -5.37202 \pm 0.74241$ arcsec

$\delta = \quad 15.22329 \pm 1.23256$ ppm

It can be seen from the Figure 11-3 that the directions and magnitudes of the post-fit residuals vary from region to region and are not random. In general, this is a frequently encountered and expected situation in conversions between two different types of networks (terrestrial and satellite-based).

The main reason for this is that the terrestrial network is subject to geometric deformations as a result of error propagation of measurement methods and the use of less accurate instruments compared to today's technology. Besides, in terrestrial networks established over a period of time spanning many years, unmodeled displacements due to crustal movements result in significant deformation in the network coordinates.

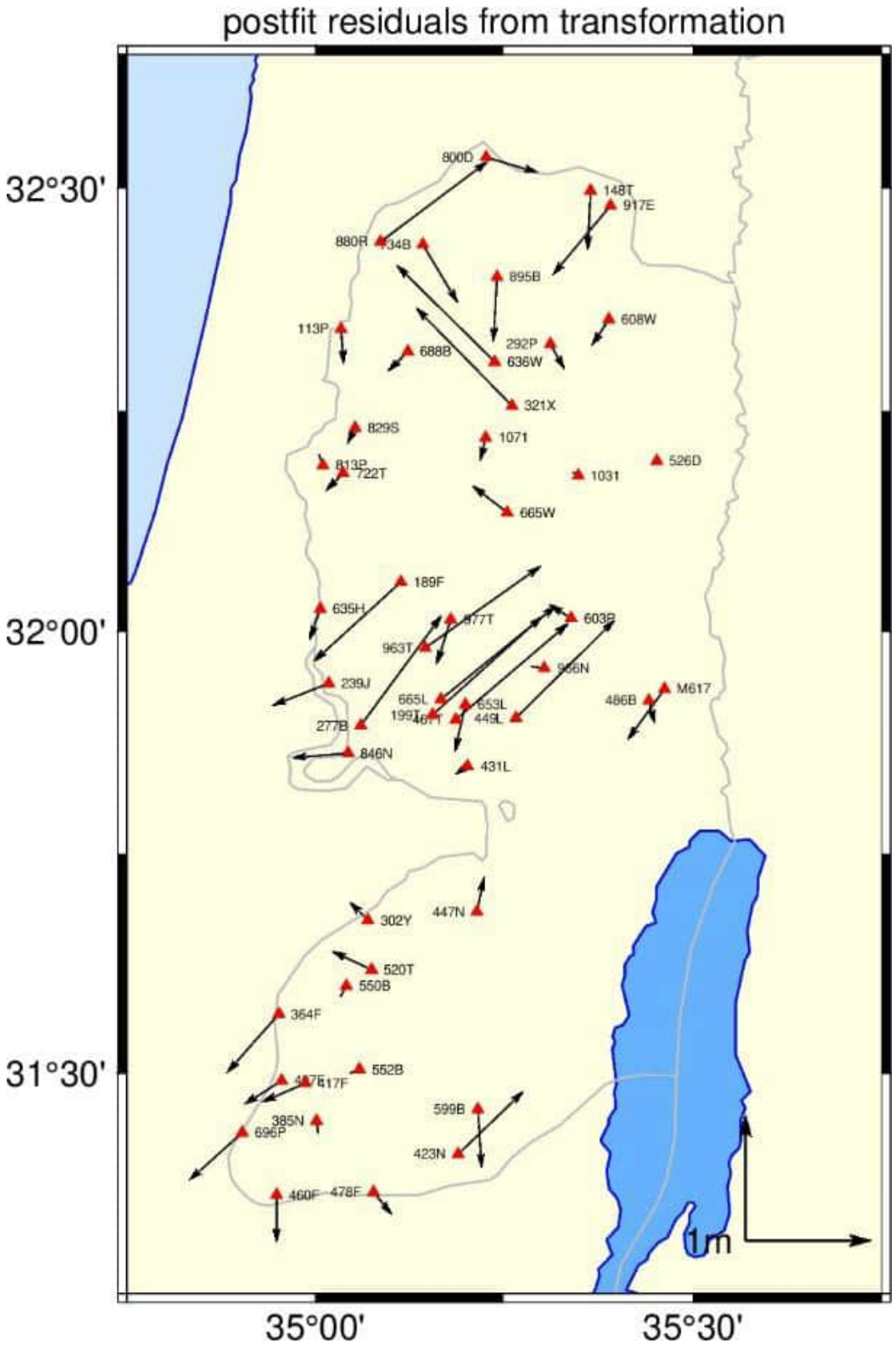

Figure 11-3: Horizontal post-fit residuals from 3D Transformation

11.2.2. Two-dimensional similarity transformation (4-parameters)

Two-dimensional similarity (Helmert) transformation is defined by four parameters and is the most commonly used planar transformation method. These four parameters are defined below and shown in Figure 11-2.

- Two translations: Δx and Δy
- A rotation: α
- A scale factor in ppm: δ

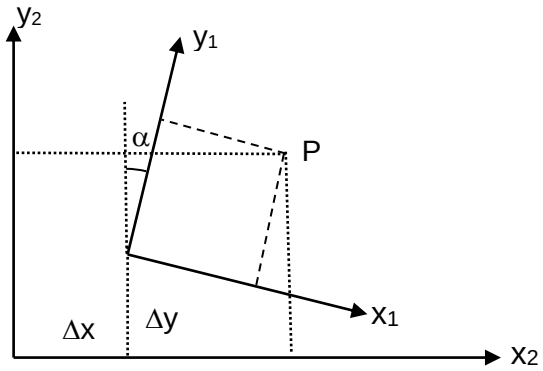

Figure 11-4: Two-Dimensional Datum Transformation

The equations are defined by

$$\begin{bmatrix} x \\ y \end{bmatrix}_2 = \begin{bmatrix} \Delta x \\ \Delta y \end{bmatrix} + (1+\delta) \begin{bmatrix} \cos\alpha & \sin\alpha \\ -\sin\alpha & \cos\alpha \end{bmatrix} \begin{bmatrix} x \\ y \end{bmatrix}_1$$

The parameters are determined by an adjustment procedure. The inverse of the transformation is set up as below:

$$\begin{bmatrix} x \\ y \end{bmatrix}_1 = \frac{1}{(1+\delta)} \begin{bmatrix} \cos\alpha & -\sin\alpha \\ \sin\alpha & \cos\alpha \end{bmatrix} \left[\begin{bmatrix} x \\ y \end{bmatrix}_2 - \begin{bmatrix} \Delta x \\ \Delta y \end{bmatrix} \right]$$

A 4-parameter Helmert transformation was applied between projection coordinates of the PAL-GRF and PAL1923. Detailed explanations about the parameters for the Cassini projection system used in PAL1923 and the Transversal Mercator systems adopted in PAL-GRF are given below. As in the 3D transformation, the 3 points mentioned above were detected as outlier and were excluded from evaluation. The parameters obtained in the two-dimensional transformation using 50 points are given below. The post-fit residuals obtained in the 2-D transformation are similar to the horizontal components of the post-fit residuals of the 3-D transformation depicted in Figure 11-3.

2D Parameters (PAL-GRF to PAL1923)

$$\Delta x = -47512.2558 \pm 0.8632 \text{ m}$$

$$\Delta y = -368390.3150 \pm 0.8632 \text{ m}$$

$$\alpha = -57.66536 \pm 0.3158 \text{ arcsec}$$

$$\delta = 11.68485 \pm 1.5309 \text{ ppm}$$

11.2.3. 2-D transformation based on coordinate differences

If both coordinate systems are homogeneous, suitable results can be obtained with three/two-dimensional similarity transformation. Especially in historical terrestrial networks, points are physically displaced due to the effects of earthquakes. In addition to the geometric reasons mentioned above, the initial states of these networks change due to physical reasons and the network loses its homogeneous character over time. In this case, it is not appropriate to model the difference between two systems with a three/two-dimensional similarity transformation.

The size and distribution of the residuals obtained in two- and three-dimensional transformation show that there are such distortions in the existing old network. Moreover, these values are not systematic pattern in different regions of the network. For this reason, it is not appropriate to divide the entire area into sub-regions and determine different transformation parameters for each sub-region.

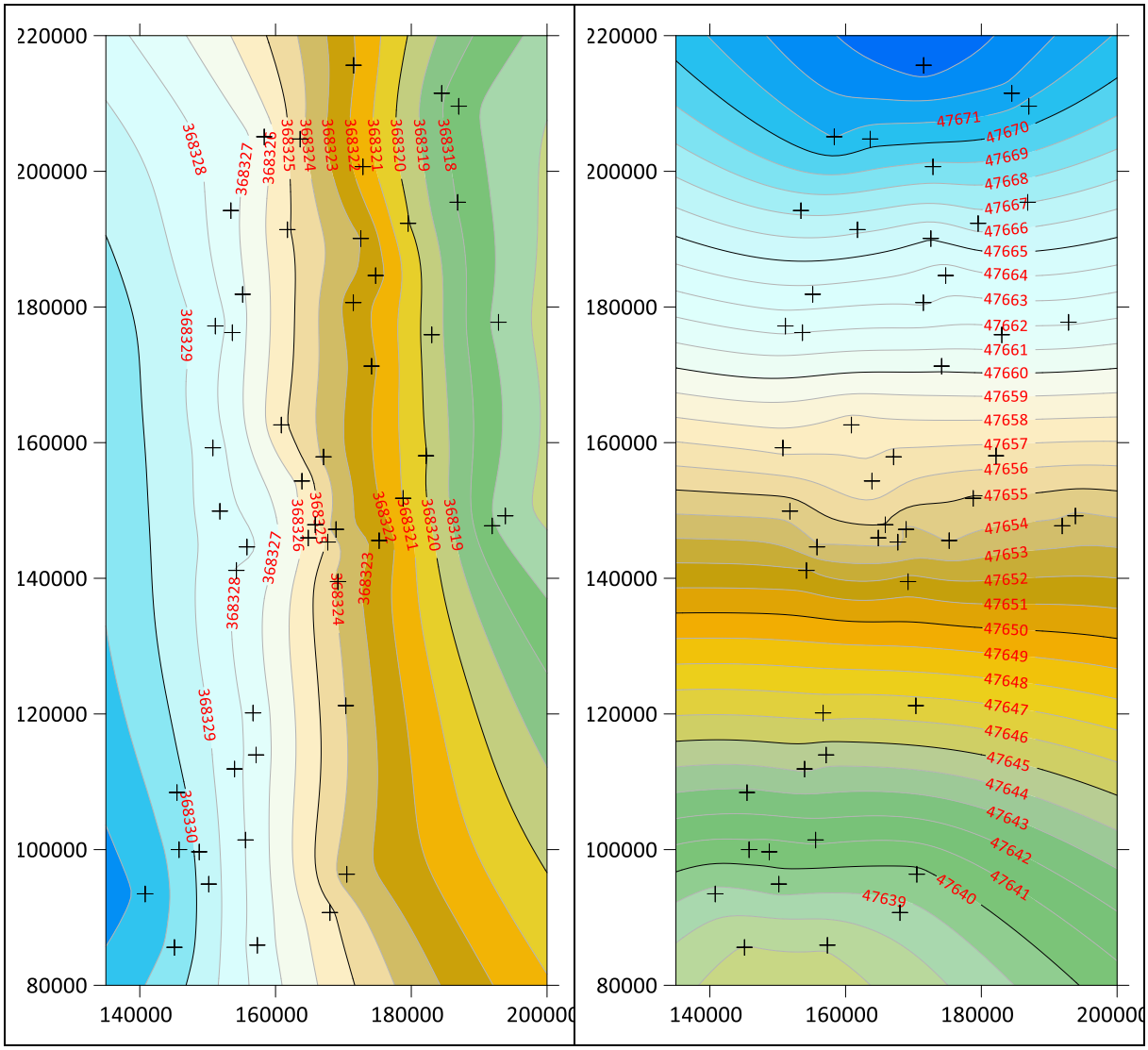

Figure 11-5: Northing and Easting Coordinate Differences in meters (PAL-GRF-PAL1923). They are used for transformation from PAL1923 to PAL-GRF.

For the transformation between these two systems, a method of coordinate differences was used. It is based on first gridding the north and east coordinate differences (dN and dE) at common points and then interpolating the differences at any point using this grid data.

The Kriging method was used separately for gridding northing and easting differences. Grid data for the conversion from PAL1923 to PAL-GRF is given in Figure 11-5, and for the inverse transformation is given in Figure 11-6. The values in these two groups of grid files are opposite signs of each other, but the coordinate axes values are related to the relevant coordinate system.

With this method it is achieved that the results adapt to local coordinate differences rather than regional as much as possible.

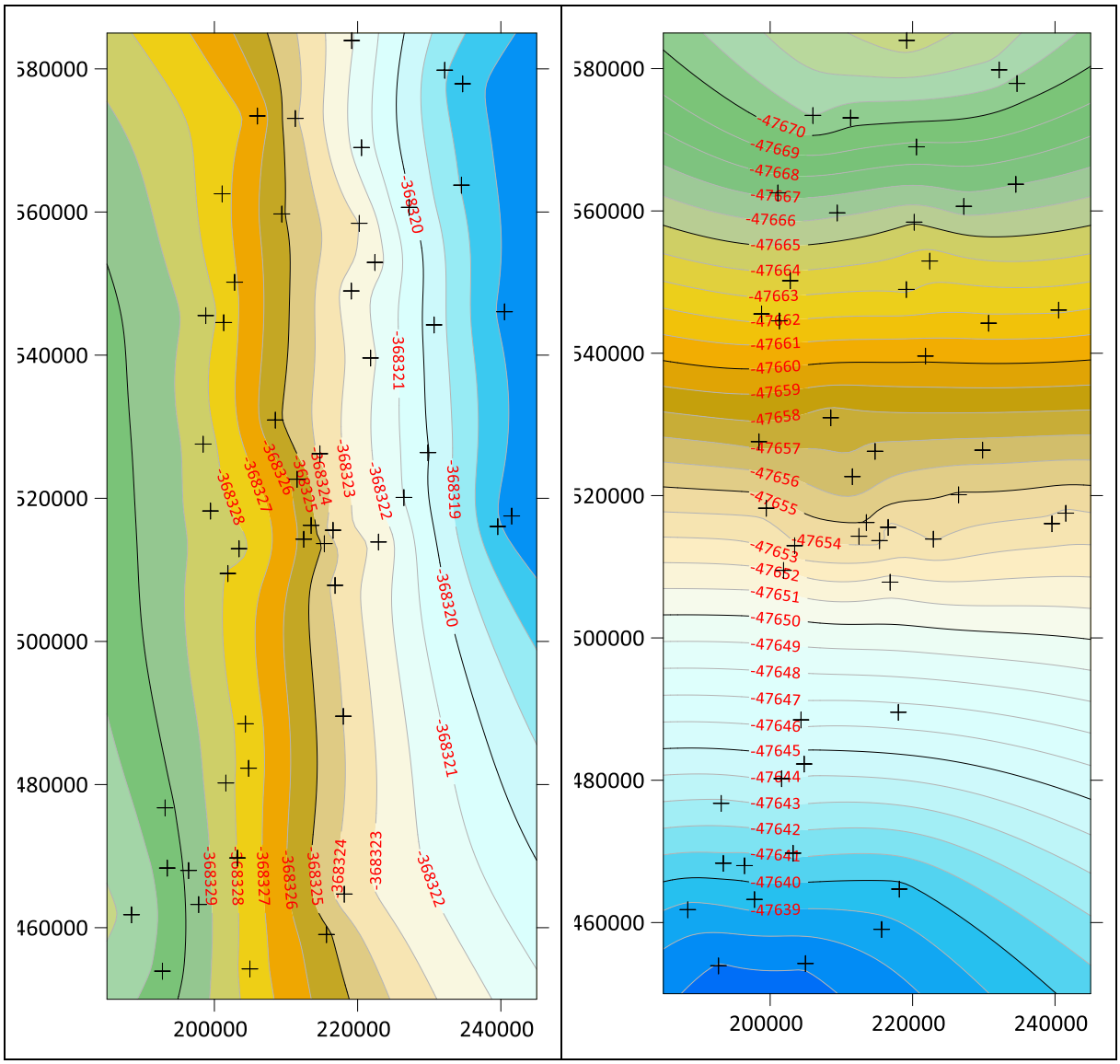

Figure 11-6 : Northing and Easting Coordinate Differences in meters (PAL1923-PAL-GRF). They are used for transformation from PAL-GRF to PAL1923.

11.3. Coordinate conversions

11.3.1. PAL1923 Grid Projection System (CASSINI SOLDNER)

Palestine 1923 Grid (EPSG: 28191), so called Israeli old grid was defined based on Cassini projection system with the parameters given in Table 11-5 below. Cassini-Soldner is a transverse cylindrical

projection system. It is equidistant along the central meridian and all lines perpendicular to it. Scale along its central meridian, and everywhere at right angles to it is true.

The equator, central meridian, and meridians 90° from the central meridian project as straight lines. Other meridians project as complex curves concave toward the central meridian and perpendicularly intersect with the equator. Other parallels are also complex curves.

Table 11-7: PAL1923 Grid Projection Parameters

Parameter	Description	Symbol
Projection	Cassini-Soldner	
Ellipsoid	Clark 1880	
Semi-major axis	6378300.789 m	a
Inverse flattening	293.466315538981	1/f
latitude of origin	31.734096944444445°	φ_0
longitude origin	35.212080555555556°	λ_0
False Easting	170251.555 m	F_E
False Northing	126867.909 m	F_N
Scale	1	k_0
EPSG code	2891	

11.3.1.1. Coordinate conversion from geodetic coordinates (φ and λ) to Cassini - Soldner projection coordinates (N, E)

The formulas to obtain the Easting and Northing projection coordinates from geodetic coordinates are:

$$\mathrm{E} = R_N \ (\mathrm{A} - \frac{\mathrm{T}A^3}{6} - \frac{(8 - T + 8C)\ T\ A^5)}{120} + F_E$$

$$\mathrm{N} = \mathrm{M} - \ \mathrm{M0} + \mathrm{N}\ \tan(\varphi)\ (\frac{A^2}{2} - \frac{(5 - T + 6C)\ \ A^4}{24}) + F_N$$

$$R_N = \mathrm{a}/\sqrt{1 - \mathrm{e}^2 \sin^2 \varphi}$$

$$\mathrm{A} = (\lambda - \lambda_0) \cos \varphi$$

$$\mathrm{T} = \tan^2 \varphi$$

$$\mathrm{C} = \mathrm{e}^2/(1 - \mathrm{e}^2)\ * \cos^2 \varphi$$

$$\mathrm{e}^2 = 1 - (1 - 1/\mathrm{f})^2$$

$$\mathrm{M} = \ \mathrm{a}\left(1 - \frac{\mathrm{e}^2}{4} - \frac{3\mathrm{e}^4}{64} - \frac{5\mathrm{e}^4}{256}\right)\varphi - \left(\frac{3\mathrm{e}^2}{8} + \frac{3\mathrm{e}^4}{32} + \frac{45\mathrm{e}^6}{1024}\right)\sin(2\varphi) + \left(\frac{15\mathrm{e}^4}{256} + \frac{45\mathrm{e}^6}{1024}\right)\sin(4\varphi) - \frac{35\mathrm{e}^6}{3072}\ \sin\ (6\varphi)$$

$$M_0 = a\left(1 - \frac{e^2}{4} - \frac{3e^4}{64} - \frac{5e^4}{256}\right)\varphi_0 - \left(\frac{3e^2}{8} + \frac{3e^4}{32} + \frac{45e^6}{1024}\right)\sin(2\varphi_0) + \left(\frac{15e^4}{256} + \frac{45e^6}{1024}\right)\sin(4\varphi_0) - \frac{35e^6}{3072}\sin(6\varphi_0)$$

Here, M is the distance from the equator to the point in question along the meridian, and M_0 is the distance from the equator to the latitude of origin along the meridian.

11.3.1.2. Coordinate conversion from Cassini -Soldner projection coordinates (N, E) to geodetic coordinates (φ and λ)

The reverse calculation steps consist of the following:

$$\varphi = \varphi' - {R_N}'\frac{\tan(\varphi')}{{R_M}'}\left(\frac{D^2}{2} - \frac{(1+3T)\,D^4}{24}\right)$$

$$\lambda = \lambda_0 + \frac{1}{\cos(\varphi')}\left(D - T\,\frac{D^3}{3} + (1+3T)\,T\,\frac{D^5}{15}\right)$$

$${R_M}' = a(1-e^2)/(1-e^2\sin^2\varphi')^{3/2}$$

$${R_N}' = a/\sqrt{1-e^2\sin^2\varphi'}$$

$$T = \tan^2\varphi'$$

$$D = (E - F_{E)}/{R_N}'$$

$$\varphi' = \mu' + \left(\frac{3e'}{2} - \frac{27e'^3}{32}\right)\sin(2\mu') + \left(\frac{21e'^2}{16} - \frac{51e'^4}{32}\right)\sin(4\mu') + \frac{151e'^3}{96}\sin(6\mu') + \frac{1097e'^4}{512}\sin(8\mu')$$

$$e' = [1-(1-e^2)^{0.5}]/[1+(1-e^2)^{0.5}]$$

$$\mu' = M'/\left(a\left(1 - \frac{e^2}{4} - \frac{3e^4}{64} - \frac{5e^6}{256}\right)\right)$$

$$M' = M_0 + N - FN$$

11.3.2. PAL-GRF Projection System (Transverse Mercator)

PLA has adopted the Transverse Mercator (TM) system for the rectangular projection coordinates to be used for the maps along with the PAL-GRF definition. The Transverse Mercator (TM) system projects geodetic coordinates onto a cylinder which is tangent to the equator and makes contact along one meridian. To minimize distortion, the earth is "rotated" within the cylinder, to bring a different meridian into contact with the cylinder, for different areas. This results in north-south bands known as zones. The true origin for each zone is the intersection of the equator and the contacting meridian (the central meridian), but a false origin is often used to avoid negative coordinates.

The Transverse Mercator projection, whose parameters are given in Table 11-6, is slightly different from the standard TM or UTM. By choosing the central meridian (longitude of origin) and latitude of origin specific to Palestine, it is aimed to keep the deformation resulting from the projection to a minimum level.

In addition, the scale factor on the central meridian was chosen to be different than 1 (slightly higher, 1+3ppm) and so that the cylinder passes tangentially to the mean sea level. Thus, it was preferred to minimize the differences between the distances on the land and on the projection surface.

Table 11-8: PAL-GRF Grid Projection Parameters

Parameter	Description	Symbol
Projection	Transversal Mercator	
Ellipsoid	GRS80	
Semi-major axis	6378137.0 m	a
Semi-minor axis	6356752.314 m	b
Inverse flattening	293.466315538981	1/f
latitude of origin	31.777777777°	φ_0
longitude origin	35.235°	λ_0
False Easting	220000 m	F_E
False Northing	500000 m	F_N
Scale	1.000003	k_0
EPSG code		

11.3.2.1. Coordinate conversion from geodetic coordinates (φ and λ) to TM projection coordinates (N, E)

The formulas to obtain the TM projection Easting and Northing coordinates are:

$$\varphi_1 = \varphi - \varphi_0 \ , \qquad \varphi_2 = \varphi + \varphi_0 \ , \qquad e^2 = 1 - (b/a)^2$$

$$R_N = k_0\, a \,/\sqrt{1 - e^2 \sin^2 \varphi} \ , \quad R_M = R_N\,(1 - e^2)/\,(1 - e^2 \sin^2 \varphi)$$

$$m = (a - b)/(a + b), \qquad h_2 = R_N/R_M - 1$$

$$A_0 = (1 + m + 5/4\, m^2 + 5/4\, m^3)\, \varphi_1$$

$$A_1 = (3\, m + 3\, m^2 + 21/8\, m^3) * \sin(\varphi_1) \cos(\varphi_2)$$

$$A_2 = (15/8\, m^2 + 15/8\, m^3) * \sin(2\varphi_1) \cos(2\varphi_2)$$

$$A_3 = (35/24\, m^3) * \sin(3\varphi_1) \cos(3\varphi_2)$$

$$p = \lambda - \lambda_0$$

$$A_4 = k_0\, b\, (A_0 - A_1 + A_2 - A_3) + F_N$$

$$A_5 = R_N/2 * \sin(\varphi) \cos(\varphi)$$

$$A_6 = R_N/24 * \sin(\varphi) \cos^3 \varphi) (5 - \tan^2 \varphi + 9\ h2)$$

$$A_7 = R_N/720 * \sin(\varphi) \cos^5 \varphi) (61 - 58 \tan^2 \varphi + \tan^4 \varphi)$$

$$N = (A_4 + p^2 A_5 + p^4 A_6 + p^6 A_7)$$

$$A_8 = R_N \cos(\varphi)$$

$$A_9 = R_N/6 * \cos^3 \varphi\ (R_N/R_M - \tan^2(\varphi)$$

$$A_{10} = \frac{R_N}{120} * \cos^5 \varphi * (5 - 18 \tan^2 \varphi + \tan^4 \varphi + 14\ h_2 - 58 \tan^2 \varphi\ h_2)$$

$$E = F_E + p\ A_8 + p^3 A_9 + p^5 A_{10}$$

11.3.2.2. Coordinate conversion from TM projection coordinates (N, E) to geodetic coordinates (φ and λ)

The reverse calculation steps consist of the following:

$$k = (N - F_N)/(k_0\ a) + \varphi_0$$

The following equations are solved iteratively until $(N - F_N - d) < 0.001$ is achieved.

$$\varphi_1 = k - \varphi_0$$

$$\varphi_2 = k + \varphi_0$$

$$A_0 = (1 + m + 5/4\ m^2 + 5/4\ m^3)\ \varphi_1$$

$$A_1 = (3\ m + 3\ m^2 + 21/8\ m^3) * \sin(\varphi_1) \cos(\varphi_2)$$

$$A_2 = (15/8\ m^2 + 15/8\ m^3) * \sin(2\varphi_1) \cos(2\varphi_2)$$

$$A_3 = (35/24\ m^3) * \sin(3\varphi_1) \cos(3\varphi_2)$$

$$d = k_0\ b\ (A_0 - A_1 + A_2 - A_3)$$

$$k = k + (N - F_N - d)/(k_0\ a)$$

Then, using the values (R_N, R_M, h_2) defined above, latitude and longitude are obtained with the following equations.

$$y_1 = E - F_E$$

$$A_4 = \tan(\varphi)/(2\ R_M R_N)$$

$$A_5 = \tan(\varphi)/(24\ R_M {R_N}^3) * (5 + 3\ \tan^2 \varphi + h_2 - 9\ \tan^2 \varphi\ h_2)$$

$$A_6 = \tan(\varphi)/(720\, R_M {R_N}^5) * (61 + 90\, \tan^2\varphi + 45\, \tan^4\varphi)$$

$$\varphi = k - {y_1}^2\, A_4 + {y_1}^4\, A_5 - {y_1}^4\, A_6$$

$$A_7 = R_N/\cos(\varphi)$$

$$A_8 = 1/(6\cos(\varphi)\, {R_N}^3) * (R_N/R_M + 2\, \tan^2\varphi)$$

$$A_9 = 1/(120\cos(\varphi)\, {R_N}^5) * (5 + 28\, \tan^2\varphi + 24\, \tan^4\varphi)$$

$$A_{10} = 1/(5040\cos(\varphi)\, {R_N}^7) *(61 + 662\, \tan^2\varphi + 1320\, \tan^4\varphi + 720\, \tan^6\varphi)$$

$$\lambda = \lambda_0 + y_1\, A_7 - {y_1}^3\, A_8 + {y_1}^5\, A_9 - {y_1}^7\, A_{10}$$

11.4. Website for Datum transformation and coordinate conversion

A website has been prepared to perform the following transformations between the newly defined PAL-GRF and the existing PAL1923 in both directions over internet.

- 3-D 7-parameter (Bursa-Wolf) transformation
- 2-D 4-parameter Helmert transform
- 2-D coordinate difference transformation

Here it is also possible to convert from geodesic coordinates to projection coordinates and vice versa. Details of the formulations used for these transformations are given above. The website can be accessed at https://apps.mipmap.nl/transformation, shown below.

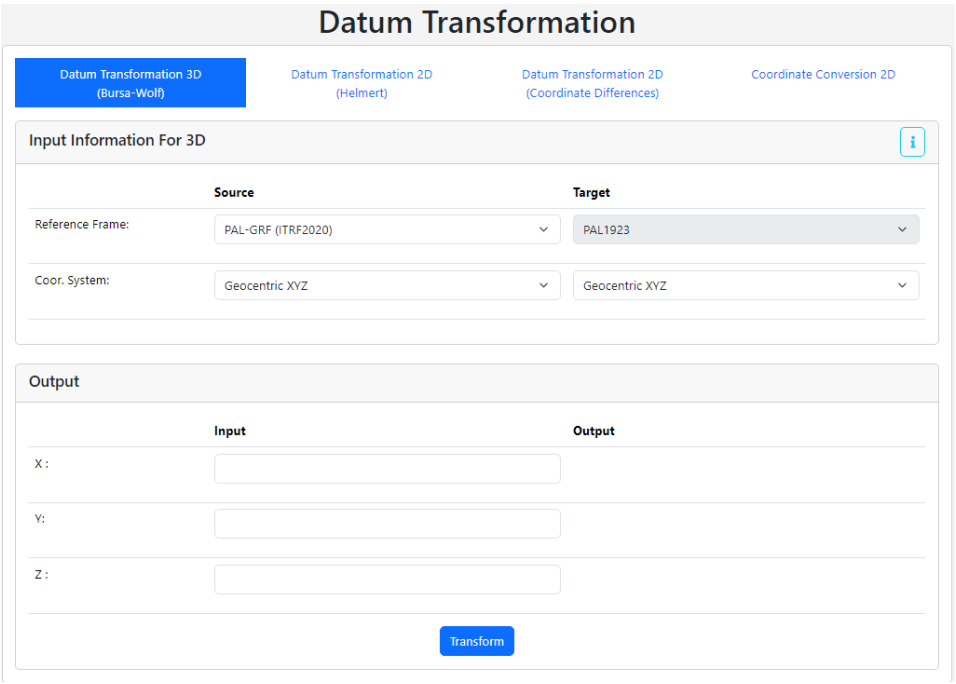

12. LOCAL GEOID MODEL AND TRANSFORMATION SURFACE FOR PALESTINE

12.1. Introduction

Orthometric (or Normal) height systems are generally used in surveying and mapping applications all over the world. Global Navigation Satellite Systems (GNSS) has been widely used in the last three decades for all kinds of point positioning. Three-dimensional coordinates of a point [Latitude (φ), longitude (λ) and ellipsoid height (h) or Cartesian coordinates (X, Y, Z)] are determined by GNSS in an earth-fixed earth-centered reference frame (e.g. ITRF, PAL-GRF). Therefore, a transformation from ellipsoidal to orthometric heights is necessary in order to obtain orthometric heights without laborious geometric leveling in the field.

The transformation between ellipsoidal and orthometric height may be directly achieved by making use of a suitable geoid model in the well-known equation ($H_P = h_P - N_P$). The well-known relations between geodetic height definitions are given in Figure 12-1 below.

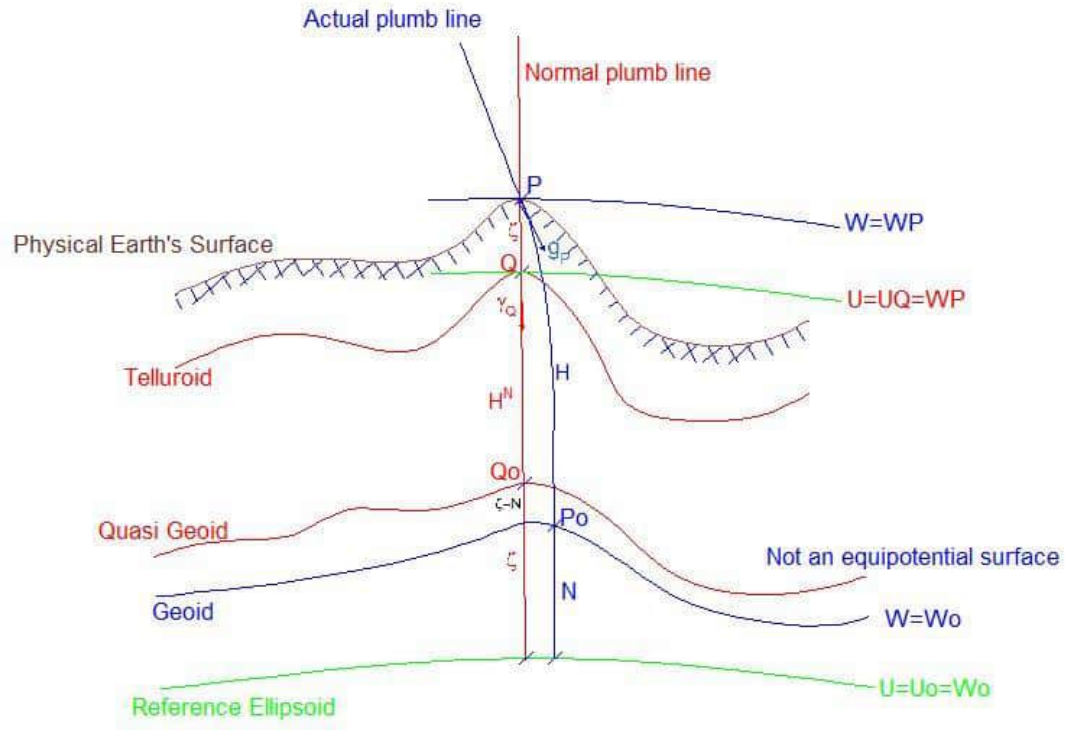

Figure 12-1: Summary of the relations between geodetic height definitions

Where;

W	:	Gravitational potential of the Earth (Actual Potential)
U	:	Gravitational potential of the reference ellipsoid (Normal Potential)
T=W-U	:	Disturbing potential
g_P	:	Actual gravity vector at point P
γ_P	:	Normal gravity vector at point Q
H	:	Orthometric Height (distance between P_0 and P)
H^N	:	Normal Height (distance between [Q_0 and P] or [Ellipsoid and Q])
N	:	Geoid height (distance between Ellipsoid and P_0)

ζ	:	Quasi-geoid height (Height Anomaly) (distance between Ellipsoid and Q_0, or distance between Q and P.
h	:	Ellipsoidal height $h_p = H_p + N_p = H_p^N + \zeta_p$ It is purely geometrical and can be directly obtained by GNSS surveying without any information on the Earth's gravitational potential
$W=W_P$	:	Equipotential surface at the surface point P
$U=U_Q=W_P$	:	Telluroid, an imaginary surface where the $W_P=U_Q$
$W=W_0$	:	Equipotential surface with $W=W_0$ (gravitational potential on the boundary surface, that is Geoid)
$U=U_0=W_0$	:	Equipotential surface in the normal potential field, with U_0 (normal potential of the reference ellipsoid). $U_0=W_0$ by definition of the reference ellipsoid.
Reference Ellipsoid		The geocentric equipotential ellipsoid (reference ellipsoid) may be defined by the following conventional constants: • equatorial radius of the Earth (a), • geocentric gravitational constant of the Earth, including the atmosphere (GM), • dynamical form factor of the Earth, excluding the permanent tidal deformation (J2), • angular velocity of the Earth (w) An equipotential ellipsoid or level ellipsoid is an ellipsoid that is defined to be an equipotential surface. If an ellipsoid of revolution (semi-major axis a, semi-minor axis b) is given, then it can be made an equipotential surface ($U=U_0$=constant) of a certain potential function U, called normal potential. This function U is uniquely determined by means of the ellipsoidal surface (semiaxes a, b), the enclosed mass M and the angular velocity ω, quite independently of the internal density distribution. The equipotential ellipsoid furnishes a simple, consistent and uniform reference system for all purposes of geodesy: the ellipsoid as a reference surface for geometric use, and a normal gravity field at the earth's surface and in space, defined in terms of closed formulas, as a reference for gravimetry and satellite geodesy. The standard theory of the equipotential ellipsoid regards the normal gravitational potential as a harmonic function outside the ellipsoid, which implies the absence of an atmosphere.
Geoid		C.F. Gauss first describes the geoid as "mathematical figure of the Earth". The equipotential surface of the Earth's gravity field which best fits, in a least squares sense, global mean sea level
Telluroid		The non-equipotential surface formed by the height anomalies from the surface of the Earth. On the telluroid, $U=U_Q=W_P$.
Quasi-geoid		An imaginary non-equipotential surface that is formed by the height anomalies from the ellipsoid similar to geoid.

A suitable geoid model with sufficient accuracy, consistent with the national height system and national vertical datum, is the straight-forward solution to the problem of the orthometric height determination directly with GNSS positioning. Otherwise, relatively time-consuming and expensive spirit-leveling would have to be carried out in all types of engineering projects. Surveyors anywhere in the world need a transformation surface that makes it possible to convert ellipsoidal heights to orthometric heights by no means of extra field work. The so-called transformation surface could be regarded as a reference surface for geo-referencing, positioning and navigation.

The data available for the computation of a local geoid model for Palestine are briefly explained below.

The Earth's Gravitational Model (EGM08) to degree and order 2160 was released to the geodetic community. EGM08 incorporates 5x5 arc-minutes gravity anomalies and has benefited from the GRACE

solutions. Improved altimetry-derived gravity anomalies and its implied Dynamic Ocean Topography model were also used in computations (Pavlis et al., 2008). The gravity anomaly and quasi-geoid height computations were achieved by using HARMONIC_SYNTHESIS software provided with the EGM08 coefficients (Holmes and Pavlis, 2006).

We used a digital terrain model (DTM) to account for terrain effects in the computations (Figure 12-2). The spatial resolution of the DTM is $3'' x 3''$ corresponding to the average distance of ~90 m between grid nodes. The elevation data were basically produced by digitizing the elevation contours of 1/250K scale topographic map sheets. We also produced the $5' x 5'$ resolution DTM for various purposes by filtering of the grid data.

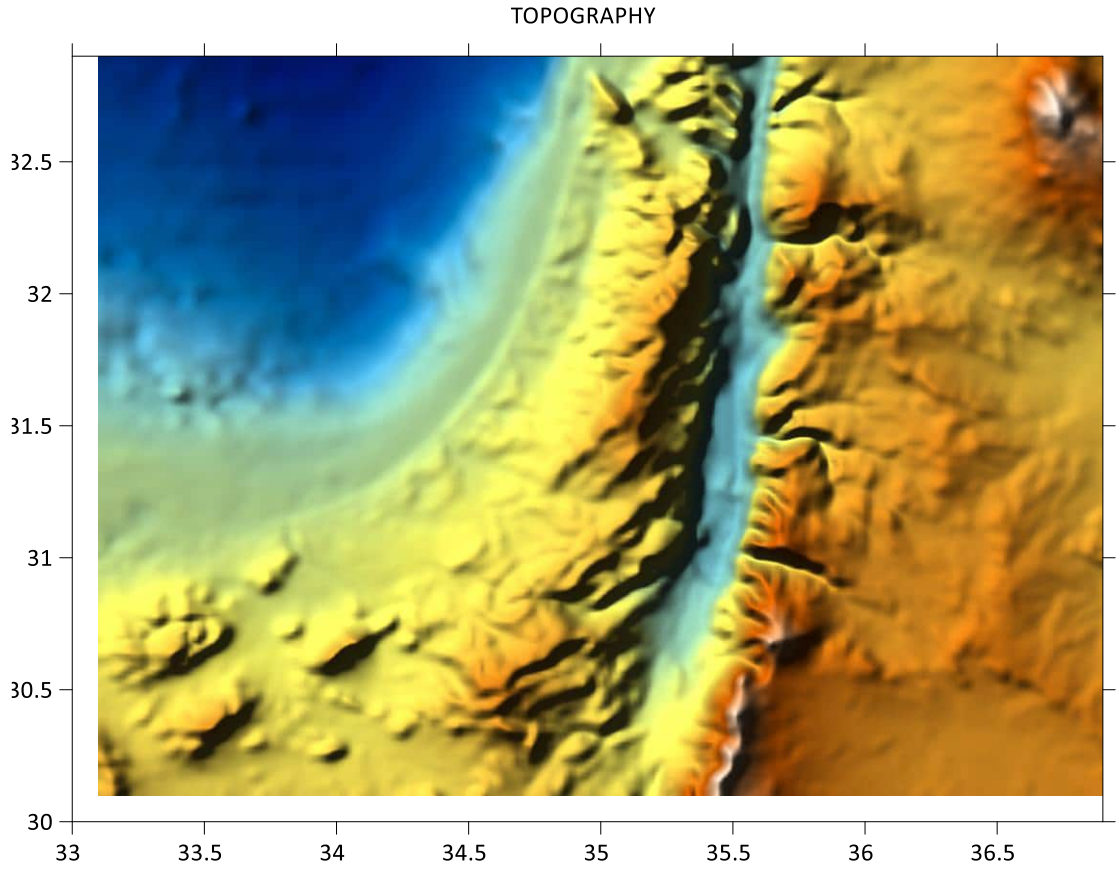

Figure 12-2: The topography of Palestine and the surrounding region as plotted in $3'' x 3''$ resolution digital terrain model. Main statistics is in meters (min: -1631.6, max: 1724.4, mean: 184.4, std.dev: 708.0). The figure shows the computation area.

12.2. Methodology for the geoid computations

The surface of the oceans, after some slight idealization, is part of a certain level surface. This particular equipotential surface was proposed as the “mathematical figure of the earth” by F.C.Gauss, and was later termed “the geoid” (Heiskanen and Moritz, 1967, p.49; Hoffmann-Wellenhof and Moritz, 2005, p.46). The geoid is still considered as the fundamental surface of the physical geodesy. In practice, we take the geoid into account during the GNSS positioning. It is well known that the difference between the orthometric height and the ellipsoidal height is called the geoid height. The geoid surface is computed with respect to the ellipsoid surface. If the geoid height is known everywhere, then the GNSS derived ellipsoidal height can simply be converted into the orthometric height by subtracting the geoid height.

The geoid height is a function of the disturbing potential, which is given as the difference between Earth's gravity potential and normal potential, and is strictly related to the fundamental equation of the physical geodesy, that links the observables (e.g. gravity) to derivatives of the disturbing potential (e.g. geoid height) as;

$$\Delta g = -\frac{2}{R}T - \frac{\partial T}{\partial r} \qquad [12.1]$$

where; Δg is gravity anomaly, T is disturbing potential, $\partial T / \partial r$ is vertical gradient of the disturbing potential and R is the radius of the Earth. Fundamental equation of the physical geodesy constitutes a Boundary Value Problem, in which geoid is the boundary surface and the gravity anomalies must be reduced to it. The gravity anomaly is the main observable to compute the geoid height with respect to an ellipsoid. Stokes formula gives a solution to the equation [12.1], and may be used to determine the geoid from the observed gravity through the combination of well-known Bruns' equation. The theory of the computation of geoid height is given in the literature in details, so that theoretical information is not given in this report.

Apart from the detailed theory, in practice, the height anomaly (quasi-geoid) can be computed by the well-known Remove-Compute-Restore (RCR) method. Moreover, the quasi-geoid can be split into three parts according to the wavelength;

$$\zeta = \zeta_{EGM} + \zeta_{RTM} + \zeta_{RES} \qquad [12.2]$$

In fact, depending on the height system used in the country, one can easily convert a height anomaly to the corresponding geoid height. Conversion from height anomaly to geoid height will be given further in this report. However, as we are stick with the data available in the computation of a local geoid model, and as we have no observed gravity for the territory of Palestine we are not able to compute the third part (ζ_{RES}), which must be computed from gravity information. Thus, the equation [12.2] becomes

$$\zeta = \zeta_{EGM} + \zeta_{RTM} \qquad [12.3]$$

Where, only the contribution of Earth's Geopotential Model (EGM) and Residual Terrain Model (RTM) will be computed in this report.

Computation of the ζ_{EGM} may be achieved through the coefficient set of an Earth's Gravitational Model (EGM) such as EGM08 (Figure 12-3). Since the observations on the Earth's surface were used in EGM computations one can compute height anomaly directly from the harmonic coefficients. In this study, we used EGM08 to degree and order 2160 to compute the ζ_{EGM} by the equation below (Holmes and Pavlis, 2006).

$$T_{EGM} = \frac{GM}{R}\sum_{n=2}^{2160}\left(\frac{R}{r}\right)^n \sum_{m=0}^{n}\left(C_{nm}\cos m\lambda + S_{nm}\sin m\lambda\right)P_{nm}(\cos\theta) \qquad [12.3a]$$

$$\zeta_{EGM} = \frac{T}{\gamma} \qquad [12.3b]$$

Where,

GM Gravitational constant and the total mass of the Earth

C_{nm}, S_{nm} Harmonic coefficients of the EGM to degree n (2160) and order m (2160)

R Mean radius of the Earth

γ Normal gravity at computation point

θ Geocentric latitude of the computation point

$P_{nm}(\cos\theta)$ Fully normalized Legendre polynomials

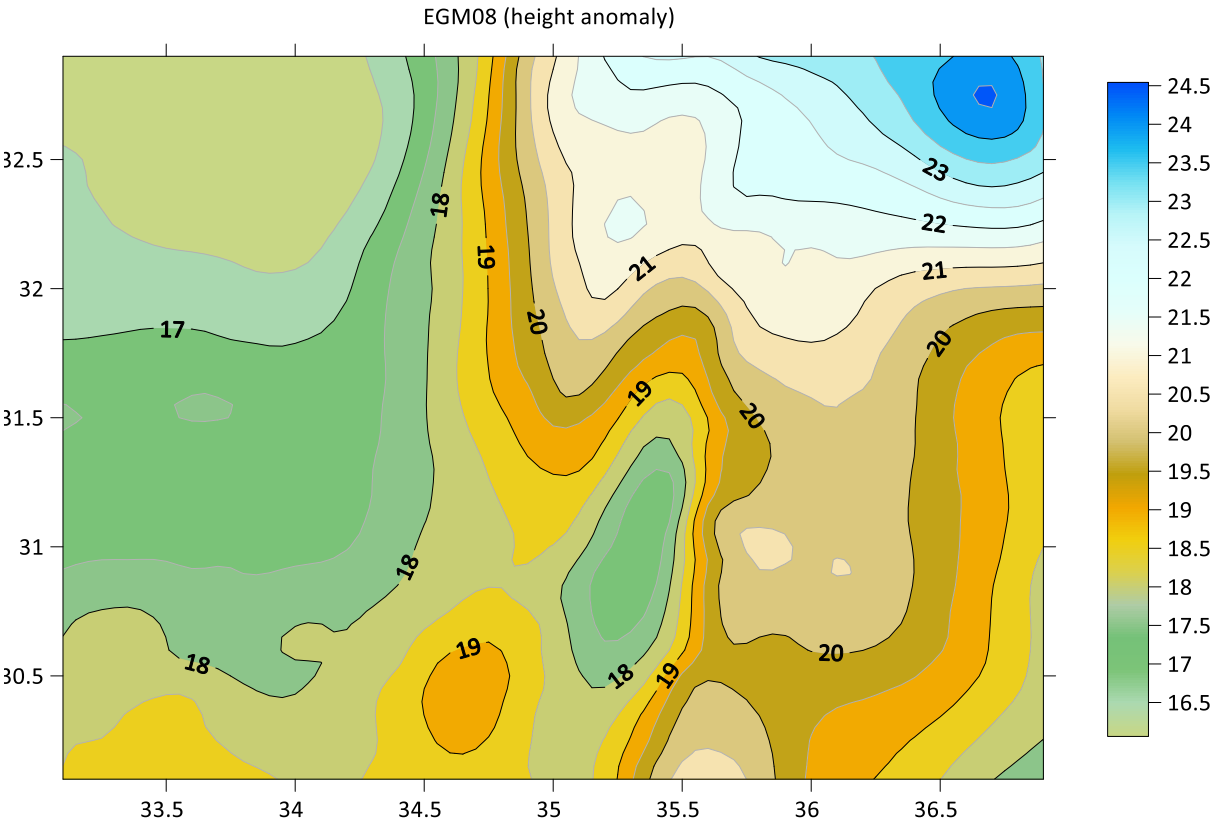

Figure 12-3: EGM08 height anomalies computed for Palestine and surrounding area in meters (min.: 16.06, max.: 24.54, mean: 19.01, st.dev: 1.87).

Actually, EGM08 fully represents the total mass of the Earth, and thus the topography above the geoid. Therefore, EGM08 derived gravity anomaly refers to the Earth's surface carrying the effect of topography to a certain resolution. It means that medium and long wavelengths of the topography have already been taken into account, but the short wavelength that is caused by the high resolution terrain. The effect of the difference between actual topography and the one used in EGM may be determined by Residual Terrain Model (RTM) (Forsberg, 1984; 1994). This is usually done by choosing a smooth reference elevation surface, and computationally removing masses above this elevation and filling up the valleys below. The reference elevation surface could be any smooth surface, and may be determined from a high resolution digital terrain model by filtering. We chose a $5' x 5'$ resolution reference surface filtered from a high resolution ($3'' x 3''$) digital terrain model. The RTM effect, here is the effect of the difference between high resolution and low resolution terrain, must be removed from the observed gravity anomaly, and then restored to computed height anomaly. Since the density anomalies (masses above and valleys below) have oscillating positive and negative values, the integrations for gravity field effects cancel each other after a suitable distance from the computation point (or outside a spherical cap with a radius selected practically). When the mean elevation surface is defined as geoid, then the RTM effect (Δg_{RTM}) corresponds to complete Bouguer reduction $(H_{REF} = 0)$ including the classical terrain correction (tc).

$$tc = G\rho \iint_{-\infty}^{+\infty} \int_{z=H_P}^{z=H(x,y)} \frac{z - H_P}{\left[(x - x_P)^2 + (y - y_P)^2 + (z - z_P)^2 \right]^{3/2}} dxdydz \qquad [12.4]$$

$$tc = G\rho \iint_{-\infty}^{+\infty} \int_{z=H_P}^{z=H(x,y)} \frac{z - H_P}{l^3} dxdydz \qquad [12.5]$$

and

$$\Delta g_{RTM} = 2\pi G\rho (H - H_{REF}) - tc \qquad [12.6]$$

Where, l is the slope distance and (x, y, z) are the coordinates of the computation and the observation (P) points. Similarly, the RTM contribution to the height anomaly may be computed as follows.

$$\zeta_{RTM} = \frac{G\rho}{\gamma} \iint_{-\infty}^{+\infty} \int_{z=H_{REF}(x,y)}^{z=H(x,y)} \frac{dxdydz}{\left[(x - x_P)^2 + (y - y_P)^2 + (z - z_P)^2 \right]^{1/2}} \qquad [12.7]$$

The above equations show that the computation of ζ_{EGM} and ζ_{RTM} is straightforward provided that harmonic coefficients and digital terrain model be available. Moreover, the problem of determination of the height anomaly reduces to the determination of the residual quasi-geoid from the residual gravity anomaly on the Earth's surface.

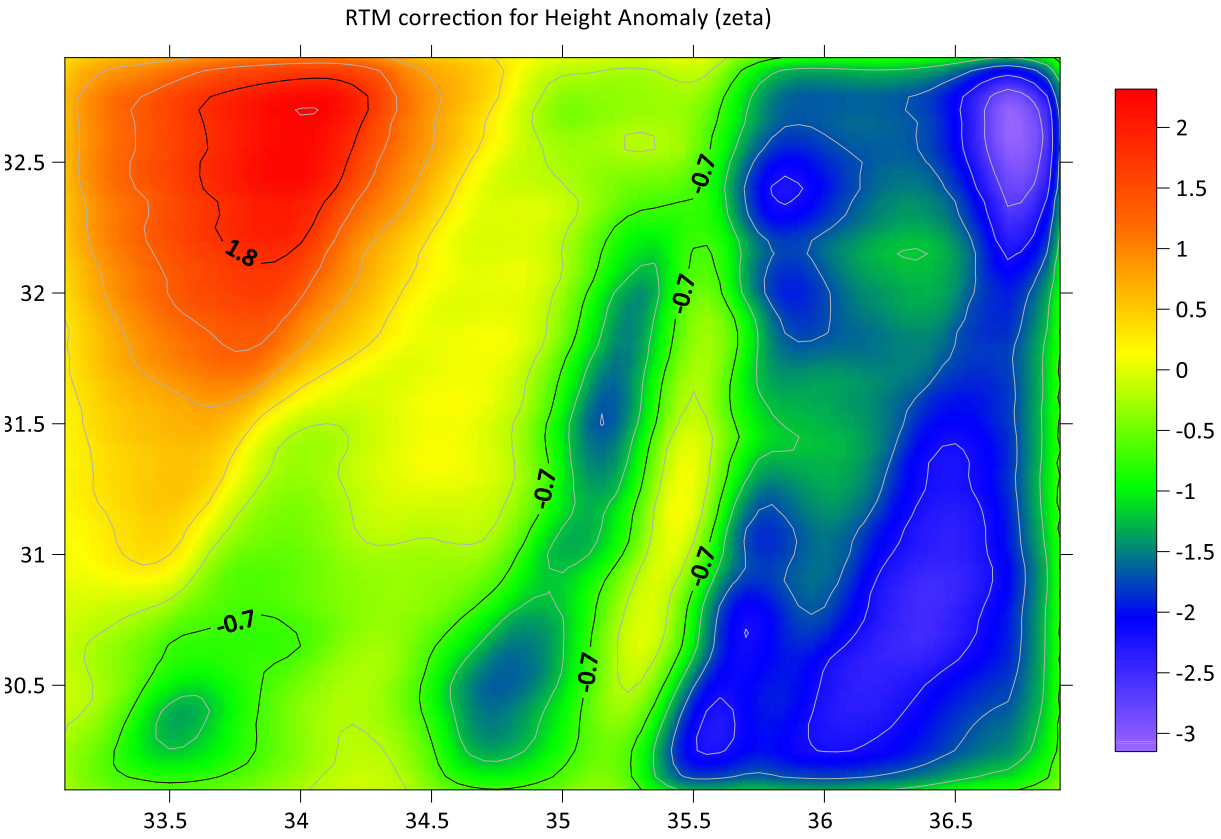

Figure 12-4: RTM height anomalies computed for Palestine and surrounding area in meters (min.: -3.15, max.: 2.32, mean: -0.59, st.dev: 1.12).

Since, we have no gravity data available we need to skip the remove ad compute steps, in which the gravity is used. Then, we may proceed with the Restore step, EGM (ζ_{EGM}) and RTM (ζ_{RTM}) contributions to the quasi-geoid heights were computed and restored to residual quasi-geoid (ζ_{RES}) so as to obtain the local quasi-geoid model (ζ_{PQG-23}). Figure 12-5 shows the final quasi-geoid model (PQG-23) after the "restore step". Table 12-1 shows the basic statistics of the data used in the "remove", "compute" and "restore" steps.

Table 12-1: Statistics of the data employed in compute and restore steps.

	ζ_{EGM}	ζ_{RTM}	ζ_{PQG-23}
	m	*m*	*m*
Minimum	16.06	-3.15	16.41
Maximum	24.54	2.32	22.99
Mean	1901	-0.59	18.42
Std.Dev.	1.87	1.12	1.28

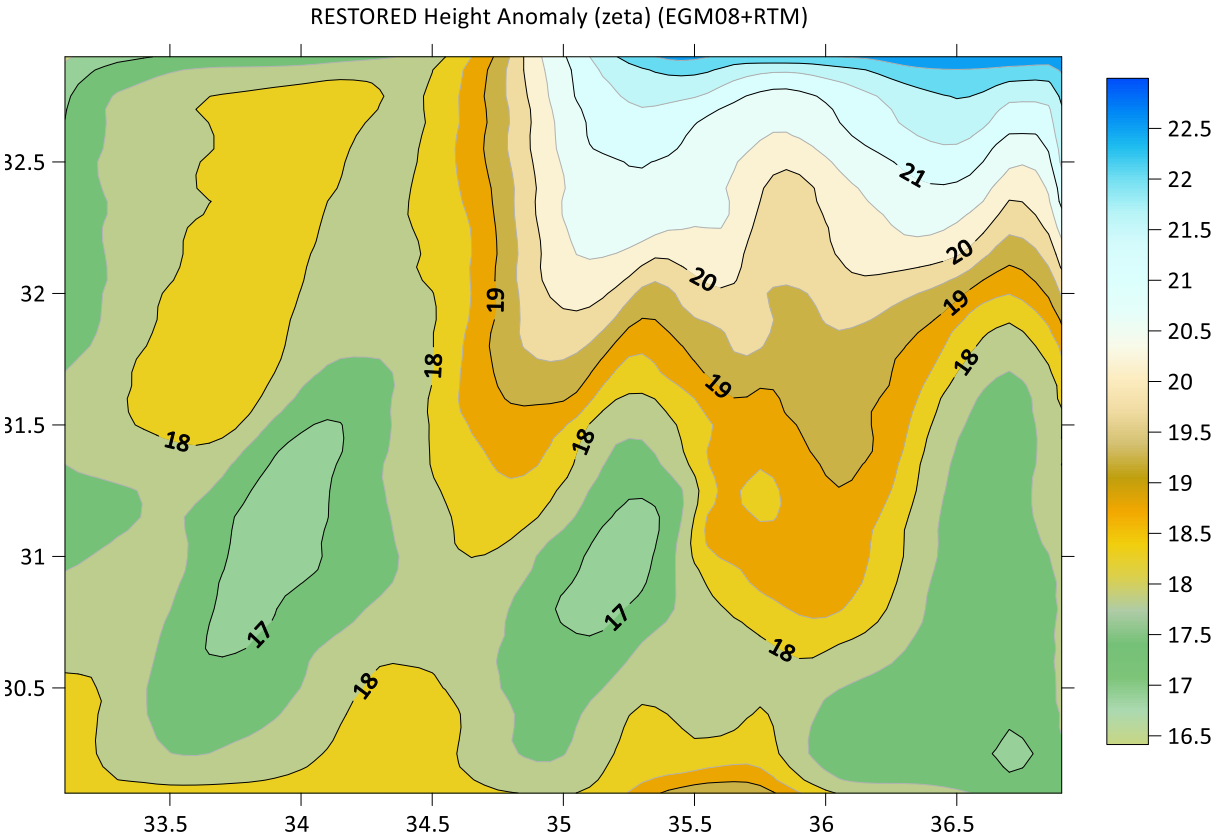

Figure 12-5: Local quasi-geoid model of Palestine (PQG-23). Computed through the sum of the individual contributions of EGM and RTM quasi-geoid ($\zeta_{PQG-23} = \zeta_{EGM} + \zeta_{RTM}$) in meters (min.: 16.41, max.: 22.99, mean: 18.42, st.dev: 1.28).

Since the Helmert orthometric height system is used in Palestine, we need to convert gravimetric quasi-geoid (PQG-23) to geoid by means of the equation below (Heiskanen and Moritz, 1967, p.327; Jekeli, 2000; Hofmann-Wellenhof and Moritz, 2005, p.327]).

$$N_{PG-23} = \zeta_{PQG-23} + \frac{\bar{g} - \bar{\gamma}}{\bar{\gamma}} H \doteq \zeta_{PQG-23} + \frac{\Delta g_B}{\bar{\gamma}} H \qquad [12.8]$$

where, $\bar{g}$ is the mean gravity along the plumb line between geoid and the ground, and $\bar{\gamma}$ is the mean normal gravity along the plumb line between ellipsoid and the telluroid. The second term in the Eq.[12.8] constitutes the correction to the quasi-geoid (PQG-23) so as to obtain the corresponding geoid model (PG-23).

The Bouguer gravity anomalies have been computed from the EGM08, and used in the equation [12.8]. The correction from ζ to N and the PG-23 geoid model are shown in Figure 12-6 and Figure 12-7 respectively.

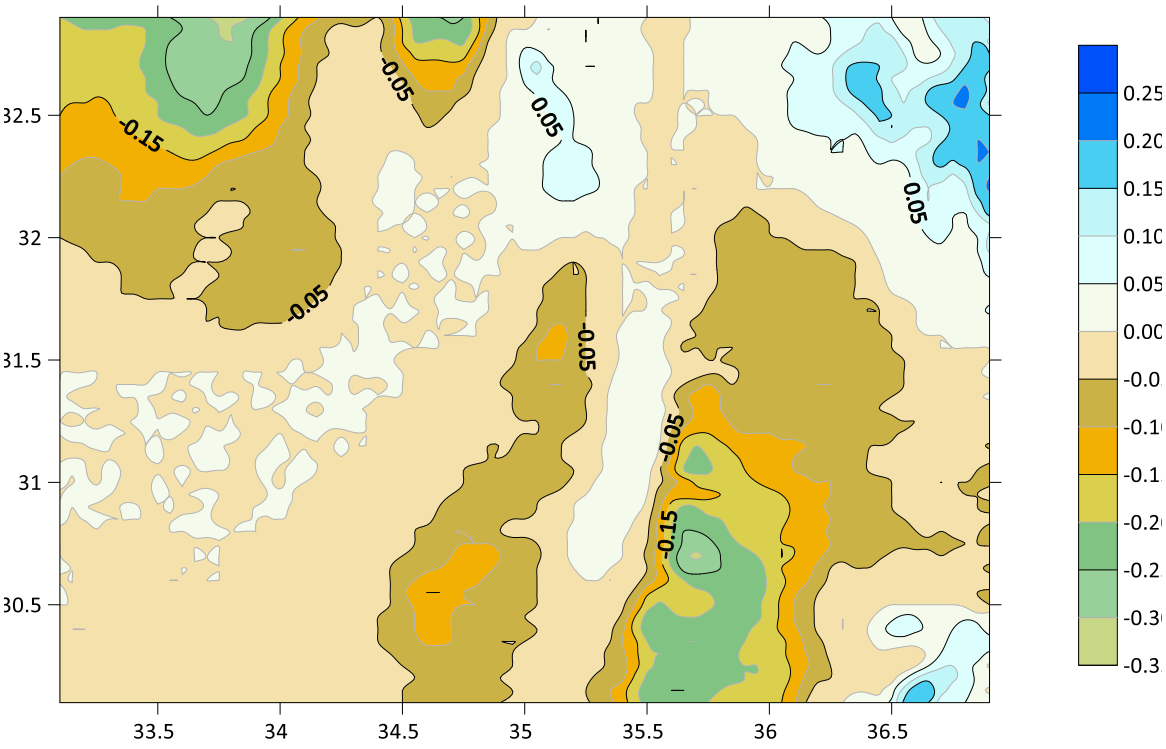

Figure 12-6: Correction model from height anomaly (quasi-geoid) to geoid height in meters (min: -0.33, max: 0.21, mean: -0.04, St.dev.: 0.08).

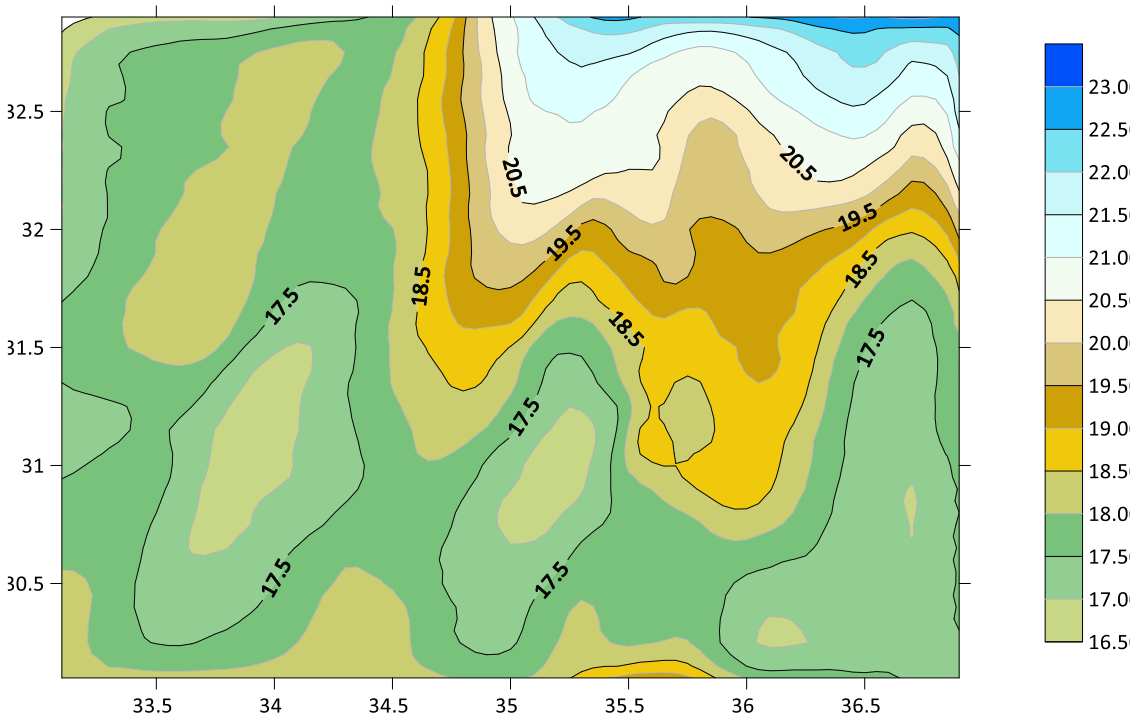

Figure 12-7: Palestine Geoid Model (PG-23). PG-23 is computed by adding the "quasi-geoid to geoid correction" to PQG-23 ($N_{PG-23} = \zeta_{PQG-23} + \frac{\Delta g_B}{\bar{\gamma}} H$) in meters (min: 16.21, max: 23.11, mean: 18.38, St.dev.: 1.31).

12.3. Combination of Palestine Geoid Model with GNSS/Lev derived geoid heights

The transformation between ellipsoidal and orthometric height may be directly achieved by making use of a suitable geoid model in the well-known equation below (Figure 12-1).

$$H_P = h_P - N_P \qquad [12.9]$$

Where, H_P, h_P, N_P are orthometric, ellipsoidal and geoid heights respectively.

Equation [12.9] requires that geoid height be known at each point with GNSS derived ellipsoidal height. Moreover, geoid height at desired point can be computed by means of interpolation from a local geoid model provided (PG-23).

Such regional gravimetric geoids, based on a global geopotential model, are computed by using local data, and thus do not contain full information of the global geopotential models. And the national vertical datum in use does not necessarily coincide with the geoid. These may cause misfit between local height system and the gravimetric geoid on long wavelengths. In order to compute a geoid model compatible with national height system, the gravimetric geoid model should be corrected by the aid of local GNSS/leveling data. The new geoid model obtained by the combination of gravimetric geoid and GNSS/leveling data defines a new reference surface to be consistently used in national height system. The number and distribution of the GNSS/leveling data assures the goodness of fit between gravimetric and GNSS/leveling geoid heights.

GNSS/leveling geoid height of a point is computed by GPS derived ellipsoidal height and the orthometric height determined by geometric leveling measurements as follows.

$$N_{GNSS/lev} = h_{GNSS} - H_{lev} \quad [12.10]$$

Ellipsoidal and the orthometric height of the point should be determined based on the national reference frame and vertical datum respectively.

12.3.1. Methodology of the combination model

After a gravimetric geoid model is computed over the Palestine (PG-23), geoid heights at desired points can be easily determined by means of interpolation methods using the gridded geoid heights. On the contrary, the points with GNSS/Lev geoid heights are sparsely distributed in the area due to laborious geometric leveling measurements. Therefore, a correction model to the gravimetric geoid should be determined in order to obtain a combined geoid to be interpolated for practical use. This correction model may also be called a 1-D transformation surface for heights.

The differences (dN) between gravimetric (N_{GRAV}) and GNSS/Lev ($N_{GNSS/lev}$) geoid heights at collocated stations are used as observations in this study.

$$dN = N_{GNSS/lev} - N_{GRAV} \quad [12.11]$$

The differences (dN) may be modeled by a polynomial as representing the trend (t) in the observations. The trend value (t_i) at each collocated station may be given as a polynomial, which defines an analytical surface and can be computed at any point in the area.

$$t_i = a_0 + a_1 x_i + a_2 y_i + a_3 x_i^2 + a_4 y_i^2 + a_5 x_i y_i + a_6 x_i^3 + a_7 y_i^3 + a_8 x_i^2 y_i + a_9 x_i y_i^2 \quad [12.12]$$

The Equation [12.12] shows a two-dimensional 10 parameter (a_j) polynomial of order 3. Where,

$$x_i = \lambda_i - \lambda_0$$

$$y_i = \varphi_i - \varphi_0$$

$$\varphi_0 = 0^o \quad [12.13]$$

$$\lambda_0 = 0^o$$

The number of unknown parameters indicates the figure of the trend surface; such as one-parameter gives a plane, 4- and 6-parameters give bilinear and quadratic surface respectively. The unknown parameters may be solved by least squares adjustment of the observation equations given by [12.13]. Moreover, the trend value at any point with coordinates (φ, λ) can be easily calculated by using the estimated parameters (a_i).

The residual observations (rN_i) are calculated by subtracting the trend (t_i) value from observations (dN_i) at collocated points.

$$rN_i = dN_i - t_i \quad [12.14]$$

The residual observations (rN_i) may be modeled and gridded by various methods such as collocation, weighted mean interpolation, kriging, polynomial regression. In this study, adjustable tension continuous curvature surface gridding algorithm given in Generic Mapping Tools 6.5 is used.

The gravimetric geoid heights (N_{GRAV}), trend values (t_i), and modeled residuals (rN_i) can be computed on selected grid nodes with coordinates (latitude, longitude and ellipsoid height). The three grid files may be added up to yield the combined geoid heights (N_{COMB}) on the same grid specified.

$$N_{COMB} = N_{GRAV} + t + rN \qquad [12.15]$$

Equation [12.15] gives a new reference surface compatible with national height system and vertical datum.

The combined geoid may be called a hybrid geoid, now, and defines a suitable reference surface for the determination of orthometric heights directly from GNSS derived ellipsoidal heights as follows.

$$H = h_{GNSS} - N_{COMB} \qquad [12.16]$$

The combination of gravimetric and GNSS/Leveling geoid heights provides a corrector surface, including the trend and the residuals, that removes the long wavelength errors in the gravimetric geoid and datum shift between geoid and national vertical datum.

The combination model given above is well implemented in GMT 6.5, and a script to achieve the combination is prepared by the project team. One may find various options for detrending and gridding of the observations in GMT.

12.3.2. Application of the combination model

The geoid model (PG-23) is given in Figure 12-7 above. We have been provided with 27 GNSS/lev stations that lie within the computation area. However, we pre-processed all the data and excluded 3 of them, which were determined as outliers with large post-fit residuals. The results of the computations with 27 points are given in Appendix-K. Moreover, we used 24 points for the resulting computations. Figure 12-8 show the GNSS/lev stations distributed in the project area. Note that the combination area is different than the geoid computation area above Figure 12-2. The geoid computation area is modified according to the GNSS/lev stations available, so that GNSS/lev stations show good distribution.

The GNSS/Lev geoid heights of 24 collocated stations were computed according to Eq.[12.10], and gravimetric geoid heights were interpolated from PG-23. The geoid height differences at 24 collocated stations were calculated (Figure 12-8), and the statistics are given in Table 12-2.

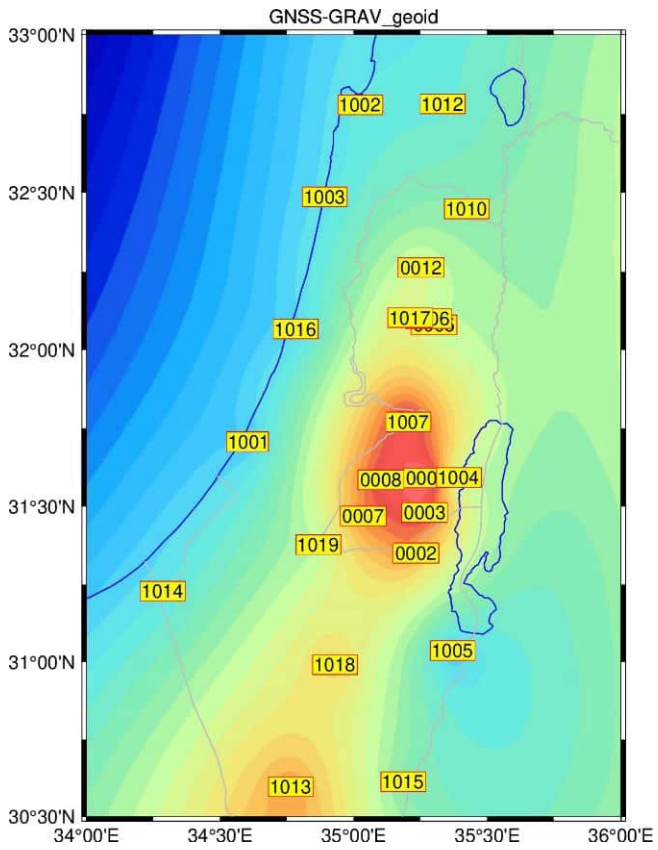

Figure 12-8: The differences (*dN*) between geoid heights at 24 collocated stations ($N_{GNSS/Lev} - N_{PG-23}$).

(Min: -1.562 m, max :2.222 m, mean: 0.257 m)

Figure 12-8 shows that some of the collocated stations in West Bank have higher differences than others. We did exclude 3 stations since we have no information about the connection measurements or accuracy of the leveling. On the other hand, we assume that some surveying projects have already been carried out depending on these stations, and the new projects depending on this geoid model should fit to the previous ones.

Table 12-2: The statistics of the geoid heights and differences at collocated stations (in meters)

	N PG-23	N GNSS/Lev	N GNSS–PG23
Number	24	24	24
Minimum	17.064	16.217	-0.846
Maximum	21.698	21.241	1.394
Mean	18.813	18.984	0.171
St. Dev.	1.389	1.352	0.699

PG-23 geoid model has been combined with 24 GNSS/Leveling geoid heights according to the model given above.

In the first step, the trend in the differences (*dN*) was computed as given in Eq.[12.12]. A re-weighted iterated robust estimation method was used for solving the unknown parameters in the polynomial. In the beginning the weights of all observations were constrained to unit matrix. This method, then, iteratively reweights the observations to reduce the influence of outliers.

Table 12-3 shows the polynomial parameters of the trend surface computed in the combination, and the trend surface is given in Figure 12-9. Trend values at ($15'' \times 15''$) grid nodes were computed.

Table 12-3: Statistics of the 10-parameter polynomial trend surface and residuals.

Longitude	Latitude	dN	Trend t	Residual dN-t	weight
35.241538	31.351956	0.546	0.874	-0.328	1
35.233166	31.350247	0.796	0.905	-0.109	1
35.265919	31.48086	1.178	0.828	0.349	1
35.273709	31.592109	1.394	0.808	0.585	0.85
35.300585	32.081054	-0.068	0.412	-0.480	0.93
35.280913	32.101255	0.029	0.401	-0.372	0.99
35.035684	31.469886	0.852	0.805	0.046	1
35.102095	31.585593	1.097	0.849	0.248	1
35.252548	32.263514	0.197	0.171	0.026	1
34.606645	31.707936	-0.733	-0.926	0.192	1
35.022984	32.778985	-0.443	-0.425	-0.018	1
34.890185	32.488254	-0.566	-0.487	-0.079	1
35.39207	31.5932	-0.114	0.136	-0.251	1
35.368823	31.036914	-0.846	-0.935	0.088	1
35.202452	31.771153	1.318	0.782	0.536	0.89
35.421613	32.449921	-0.215	-0.299	0.084	1
35.331446	32.782496	-0.457	-0.584	0.127	1
34.763139	30.597605	0.808	0.590	0.217	1
34.283821	31.228182	-0.532	-0.480	-0.051	1
35.18395	30.613631	-0.266	-0.217	-0.048	1
34.780897	32.067996	-0.697	-0.704	0.007	1
35.20967	32.103833	0.365	0.362	0.002	1
34.928268	30.991569	0.543	0.924	-0.380	0.99
34.86631	31.377823	-0.070	0.210	-0.280	1
Statistics	**Min.**	**-0.846**	**-0.935**	**-0.480**	
	Max.	**1.394**	**0.924**	**0.585**	
	Mean	**0.171**	**0.166**	**0.004**	
	St. dev.	**0.699**	**0.637**	**0.273**	

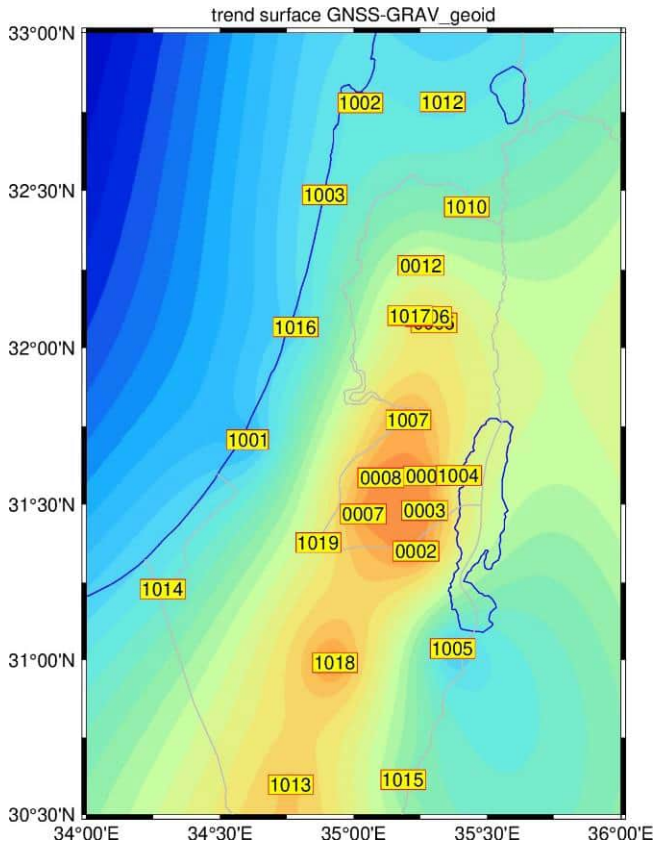

Figure 12-9: Trend surface computed in the combination.

(Min: -0.935 m, max :0.924 m, mean: 0.166 m, St.dev: 0.637 m)

10-parameter polynomial trend surface

Model Coefficients:

0.547953903696

-1.583575846910

1.714155878300

-2.278654921390

0.426925772013

0.392237960400

-0.772588695150

2.307833206910

-1.750226298160

0.236371212708

The residual geoid heights as given in Eq.[12.14] were then computed by subtracting the trend value from the geoid height difference at collocated points, and of which the statistics are shown in Table 12-3. The resulting grid file of PHG-23 is given in Appendix-K.

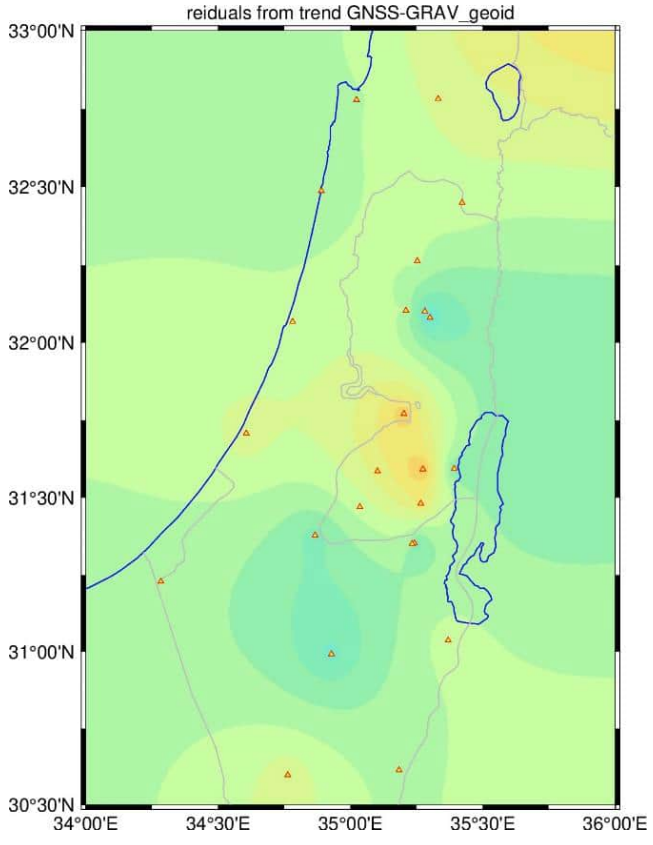

Figure 12-10: Residuals from the trend surface computed in the combination.

(Min: -0.480 m, max :0.585 m, mean: -0.004 m, St.dev: 0.273 m)

The residual geoid heights (rN_i) were then gridded by making use of adjustable continuous curvature surface gridding algorithm, implemented in GMT.

The sum of trend and modeled residuals at the same grid structure yields a corrector surface to be added to gravimetric geoid model in order to obtain the combined geoid model.

The standard deviation of the residuals indicate the precision of the prediction that can be achievable with the data available.

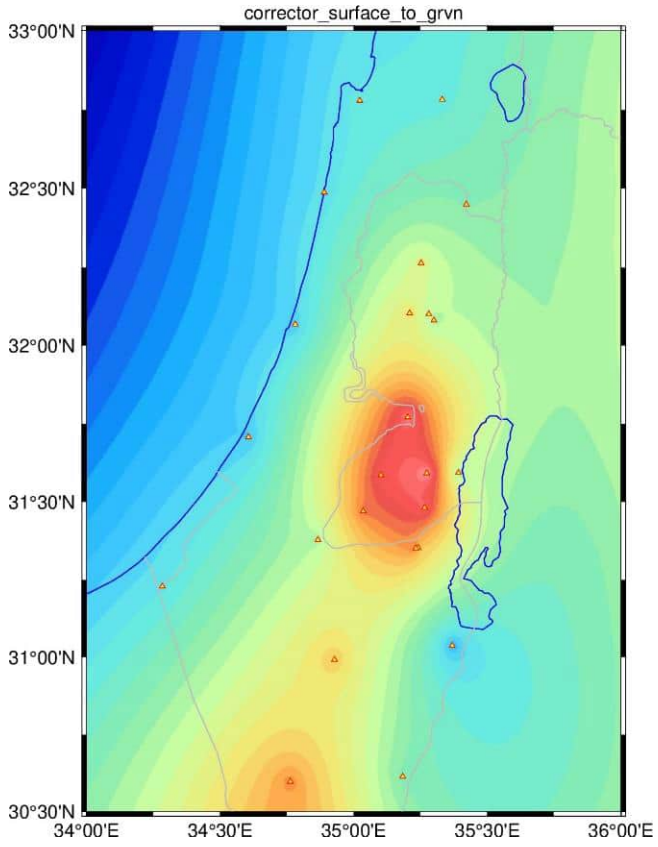

Figure 12-11: Corrector surface to gravimetric geoid (PG-23) computed by adding trend and modeled residuals.

(Min: -1.802 m, max :2.202 m, mean:-0.315m, St.dev:0.544m)

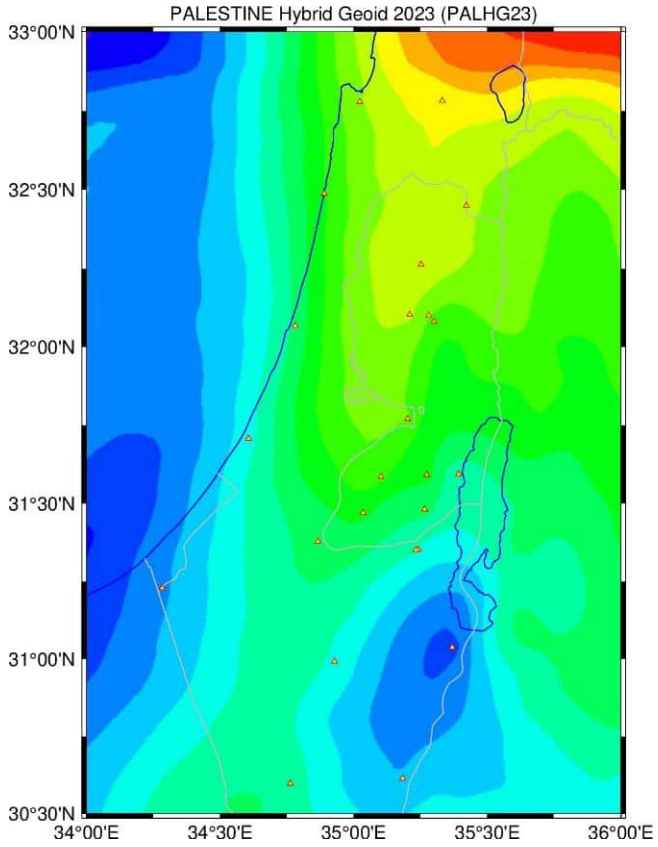

Figure 12-12: Palestine combined hybrid geoid model (PHG-23) computed by adding up gravimetric geoid (PG-23), trend and modeled residuals.

(Min: 15.472 m, max: 22.830 m, mean: 18.458 m, St.dev: 1.483m)

Gravimetric PG-23 and GNSS/Lev geoid heights have been combined using the method described above in order to provide users with a reference surface for orthometric height determination directly by GNSS in accordance with the national height system and vertical datum (PHG-23). PHG-23 should be used in the borders shown in the figure only.

12.4. Results

In this project, we basically computed a local geoid height model for Palestine with a simplified remove-compute-restore method following the Molodensky approach, in order to be used in practical surveying applications.

First we computed a quasi-geoid model based on the EGM08 and RTM. Then we converted quasi-geoid to geoid by making use of the EGM derived gravity anomalies, and finally combined resulting geoid with GNSS/Leveling geoid heights in order to obtain a transformation surface, that may be called Palestine Hybrid Geoid (PHG-23) to be used for direct computation of orthometric heights from ellipsoidal heights. Since no gravity data have been used in this computation, the computed model PHG-23 is a transformation surface that may be used for surveying applications in practice. The number of collocated stations with gravimetric and GNSS/Lev geoid heights plays an important role in the precision and accuracy of the final combined geoid. Internal check of the combined geoid would be the statistics of the residuals given in Table 12-3. Accuracy of the PHG-23 may be computed making use of extra GNSS/lev stations that were not used in the computations. After the computations the post-fit residuals ($N_{PHG-23} - N_{GNSS/Lev}$) at collocated stations must be computed. Since we do not have extra stations in our case we have no result for external check. Actually, we have two data sets in hand and no additional information which one is more correct than the other one. That's why we used all 24 GNSS/Lev stations.

While all these are geoid-like surfaces, none of them are the same. The term transformation surface reflects the fact that this is neither a geoid nor a quasi-geoid, but a surface designed to establish a base for the Palestine Vertical Control Network. Since the classical vertical control networks are not expected to be re-observed/revised in the near future, it is necessary to establish a vertical datum even for practical purposes.

We believe that the determination of an accurate geoid model cannot be achieved with the models and data given in this study. However, the theory, data collection and computer capability are improving so rapidly that such an objective for Palestine could be feasible in the future. The actual accuracy, of course, depends on the available data, their accuracy and their spatial distribution.

13. CONCLUSIONS

The project “Development of National Palestinian Geodetic Reference Framework (PAL-GRF)” is a sub-component (2.2) of the “West Bank & Gaza Real Estate Registration Project (RERP)”, which is being carried out with the financial support of the World Bank.

PAL-GRF is implemented under the responsibility of Palestine Land Authority (PLA), the national agency responsible for property registration and related transactions, including transfers and mortgages, and state property management.

Geodetic positioning is the determination of the geometrical coordinates with respect to the Earth’s geometry, and physical heights with respect to the Earth’s gravitational potential field. Positioning tasks should be referenced to a national Palestine Geodetic Reference Frame (PAL-GRF). PAL-GRF has been defined with respect to the International Terrestrial Reference Frame (ITRF), which is endorsed by the IUGG. The PAL-GRF will provide this common geodetic positional system, the foundation for using geospatially referenced data and cost-effective sharing of governmental data resources, to form the digital framework of the NSDI.

This report describes the GNSS measurements and pre- and post-processing of the data, which were carried out within the establishment of the PAL-GRF.

PAL-GRF network consists of 10 local stations and all the GNSS observations were carried out by the PLA staff. PAL-GRF stations were observed three/four times, while each observation session lasted at least 8 hours. All of the GNSS observations were converted to RINEX format for further computations.

We processed the GNSS data from doys_158-184-198-207 with the TEQC software. The summary of the teqc execution evidently shows that all the GNSS data collected at PAL-GRF stations are in good condition and quality to be used in further processing.

In addition to the PAL-GRF stations, RINEX data from IGS and IGS/ITRF stations were obtained. All the GPS&GLONASS data from all stations were processed using the same processing strategy applied before with CODE Analysis Center standard products by making use of Bernese GNSS Software V5.2.

All the GNSS data were processed on a daily basis, considering a whole day as a single session. Least Squares Estimation theory was applied in all processing steps. Moreover, loosely constrained daily normal equation systems (NQ0), which consists station coordinates only, were computed and stored. The so-called loosely constrained solutions will be used, in the future, for the combination of epoch wise solutions and estimation of the station coordinates as well as their associated velocity field.

Daily repeatability of all stations was computed and then, all daily loosely constrained solutions were combined with a suitable geodetic datum definition so as to obtain coordinates of stations in ITRF2020 (2023.50) and also loosely constrained campaign solution.

As a result of this work, the coordinates of 10 stations have been computed in ITRF2020 (at 2023.50) so as to establish the first realization of the Palestinian Geodetic Reference Frame (PAL-GRF).

To determine the velocities (yearly coordinate changes) at PAL-GRF stations, we post-processed 3 years of continuous GNSS data collected at 50 CORS stations located in the vicinity of the country. Then velocity field of the country was determined by performing time series analysis of daily solutions. Based on this velocity field, the velocities at the PAL-GRF points were estimated. Since the relative movement of PAL-GRF stations is almost less than 1 mm/year and is practically insignificant, it was concluded that a static datum definition would be appropriate for PLA-GRF. As a result, PAL-GRF is defined in ITRF2020 in the 2023.5 epoch, but for different epochs, PAL-GRF coordinates deviate from ITRF2020 due to crustal movements.

Datum transformations in 3-D and 2-D between PAL-GRF and old Palestinian datum have been applied and transformation parameters are determined for practical use.

Further this project, we basically computed a local hybrid geoid model for Palestine (PHG-23) with a simplified remove-compute-restore method following the Molodensky approach, in order to be used in practical surveying applications.

14. REFERENCES

Altamimi, Z., Rebischung, P., Collilieux, X., Métivier, L., Chanard, K. (2022): ITRF2020 [Data set]. IERS ITRS Center Hosted by IGN and IPGP, https://doi.org/10.18715/IPGP.2023.LDVIOBNL

BÖHHBÜY (2018): Büyük Ölçekli Harita ve Harita Bilgisi Üretim Yönetmeliği. Yayımlandığı Resmî Gazetenin Tarihi : 26/6/2018 No : 30460 Mükerrer. (https://www.mevzuat.gov.tr/MevzuatMetin/3.5.201811962.pdf).

Brockmann, E. (1997): Combination of Solutions for Geodetic and Geodynamic Applications of the Global Positioning System (GPS), Band 55 in der Reihe der Schweizerischen Geodätischen Kommission.

Chen, Y., and Z. Yang (**) : A hybrid method to determine the Hong Kong geoid.

Dach, R. et al. (2015): Bernese GNSS Software Version 5.2, Astronomical Institute, University of Bern, (http://www.bernese.unibe.ch/docs/DOCU52.pdf)

EPN_CB (2010): Guidelines for the EPN Analysis Centres. EUREF, IAG.

FGCC (1984): Standards and specifications of for Geodetic Networks, NGS,NOAA.

FGCC (1988): Geometric Geodetic Accuracy Standards and Specifications for using GPS Relative Positioning Techniques.

Gomez, F. et al. (2007): Global Positioning System measurements of strain accumulation and slip transfer through the restraining bend along the Dead Sea fault system in Lebanon. Geophys. J. Int. 168 (3): 1021–1028.

Grebenitcharsky, R., P. Dimitrov, L. Pashova, E.V. Rangelova (2000): A comparison of gravimetric geoid to GPS/leveling derived quasi-geoid in a small test area. Paper presented in IAG International Symposium on Gravity, Geoid and Geodynamics 2000, July 31- August 4, Banff, Alberta, Canada.

Haddad, A. et al. (2019): Tectonics of the Dead Sea Fault Driving the July 2018 Seismic Swarm in the Sea of Galilee (Lake Kinneret), JGR Solid Earth, 10.1029/ 2019JB018963. “Figure 4: GPS relative velocity field around the region (Arabian versus African, mm/yr)”

IGS Central Bureau (2015): IGS Site Guidelines, cb@igs.org (https://www.igs.org/wp-content/uploads/2019/08/IGS-Site-Guidelines-July-2015.pdf).

Kılıçoğlu, A. and O. Fırat (2003): Geoid modeling and applications for the determination of orthometric heights in large scale map production (in Turkish), Proceedings of the GIS and Geodetic Networks Workshop, Turkish National Geodesy Commission, 24-26 September, Selçuk University, Konya.

Koch, K.R., (1987): Parameter Estimation and Hypothesis Testing in Linear Models, Springer-Verlag, New York.

Kuroishi, Y., H. Ando, Y. Fukuda (2002): A new hybrid geoid model for Japan, GISGEO2000, Journal of Geodesy, Vol.76, No.8, pp:428-436.

Montenbruck O, Schmid R, Mercier F, Steigenberger P, C, Fatkulin R, Kogure S, Ganeshan AS (2015) GNSS satellite geometry and attitude models. Adv Space 56(6): 1015-1029, doi: 10.1016/j.asr.2015.06.019

Najkagawa, H., K. Wada, T. Kikkawa, H. Shimo, H. Andou, Y. Kuroishi, Y. Hatanaka, H. Shigematsu, K. Tanaka, Y. Fukuda (2003): Development of a New Japanese Geoid Model, "GSIGEO2000", Bulletin of GSI, Vol. 49.

Ostini, L., R. Dach, M. Meindl, S. Schaer, and U. Hugentobler (2008): FODITS: A new tool of the Bernese GPS Software. In Torres, J. A. and H. Hornik, editors, Subcommission for the European Reference Frame (EUREF).

Rothacher M, Schmid R (2010): ANTEX: The Antenna Exchange Format, Version 1.4(ftp://igs.org/pub/station/general/antex14.txt)

Schmid R, Dach R, Collilieux X, Jaeggi A, Schmitz M, Dilssner F (2016): Absolute IGS antenna phase center model igs08.atx: status and potential improvements. J Geod 90(4): 343-364, doi: 10.1007/s00190-015-0876-3

Wessel, P., Luis, J. F., Uieda, L., Scharroo, R., Wobbe, F., Smith, W. H. F., & Tian, D. (2019): The Generic Mapping Tools version 6. *Geochemistry, Geophysics, Geosystems*, 20, 5556–5564. https://doi.org/10.1029/2019GC008515.

15. APPENDICES

15.1. PAL-GRF Computations

15.1.1. (A) Daily Measurement Log Sheets

15.1.2. (B) Quality Check of observations at PAL-GRF stations

15.1.3. (C) PAL-GRF - Rinex Data of Local Network Stations

15.1.4. (D) PAL-GRF - Rinex Data of IGS and ITRF2020 Stations

15.1.5. (E) IGS Process Files

15.1.6. (F) Daily Normal Equations (NEQs)

15.1.7. (G) Network Adjustment Results

15.1.8. (H) Daily Repeatabilities

15.1.9. (I) Time series Analysis of the CORS Stations Around

15.2. (J) Datum Transformations

15.3. (K) Geoid Computation Results